Rockbursting Properties of Kimberlite – Diavik Diamond Mine Case Study

by

Paul Leveille

A thesis submitted in partial fulfillment of the requirements for the degree of

Master of Science

In Mining Engineering

Department of Civil and Environmental Engineering
University of Alberta

Abstract

Rockbursts have been a hazard for mining operations since underground mining first came into practice; the consequences they present to mining personnel and machinery can be fatal and costly. Underground mining in Northern Canada has presented the opportunity to study the bursting properties of kimberlite. Very little research has been done to determine the likelihood of kimberlite bursting, mostly because the diamond mines in Canada have been primarily surface operations. However, as the mining of diamonds in Canada has moved underground and continues to delve deeper, bursting has become a suspect for the cause of recent failures.

Six different types of kimberlite from Diavik Diamond Mine were collected and the physical properties determined by uniaxial compressive strength tests, Brazilian tensile strength tests, and cyclic loading tests. The rockburst profile for each rock type was determined based on three qualitative bursting indices developed from studies done on granite and coal. The bursting indices utilized in this study were the strain energy index, strain energy density index, and rock brittleness index. A combined rating system was created to quantify the indices, in order to compare and map the relative bursting potential of each rock type. From the combined rating system it was found that the rockbursting nature of kimberlite is not uniform, and is highly dependent on the composition and characteristics of the kimberlite present.

This research presents an initial investigation into the rockbursting potential of kimberlite. While, the applicability of the findings is limited due to the relatively small sample size, it does confirm the suspicion of the rockbursting potential in kimberlite.

Preface

This thesis is an original work by Paul Leveille; the thesis has not been published in full or part previously. The information gathered during the research for this thesis is part of a collaborative effort championed by Professor Derek Apel at the University of Alberta and Jan Romanowski from Rio Tinto's Diavik Diamond Mine to better understand kimberlite deposits.

Dedication

This thesis is dedicated to my parents, Peter and Sue Leveille, for their support during my graduate studies.

Acknowledgements

There are several groups and people that were integral to the research for this thesis. The following list is ordered based on associated group and does not represent level of importance or involvement.

Ali Sepehri, University of Alberta – Research Partner

Professor Derek Apel, University of Alberta – Supervisor

Professor Jozef Szymanski, University of Alberta – Co-Supervisor

Professor Rick Chalaturnyk, University of Alberta – Coring Equipment

Cam West, University of Alberta – Lab Technician

Greg Miller, University of Alberta – Lab Technician

Gus Fomradas, Diavik Diamond Mine, Rio Tinto – Industry Contact

Jan Romanowski, Diavik Diamond Mine, Rio Tinto – Industry Supervisor

Olga Druecker, Diavik Diamond Mine, Rio Tinto – Industry Contact

Table of Contents

List of Figures

List of Tables

List of Symbols

W_{ET} Strain energy storage index

Φ_{sp} Strain energy retained

Φ_{st} Strain energy dissipated

SED Strain energy density index (MPa)

σ_c Uniaxial compressive strength (MPa)

σ_T Tensile strength (MPa)

σ_θ Tangential stress (MPa)

E Young's modulus of elasticity (GPa)

E_s Unloading elastic modulus (MPa)

B Rock brittleness index

T_s Tangential stress index

Glossary of Terms

Term	Definition
ASTM:	American Society for Testing and Materials
Compressometer:	Device used for measuring the changing radial and axial sample length during a compression test
Geophone:	Instrument capable of detecting the movement of the ground
Hysteresis Loop:	The unloading and loading cycle on a stress-strain graph describing the loss in energy caused by friction and or fracture
Kimberlite:	A type of rock which can potentially be diamond bearing
LVDT:	Linear voltage differential transducer, used for measuring changes in length

Rock Brittleness:	Rockburst predicting method based on a ratio of the tensile and compressive strengths of a rock
Rockburst:	Instantaneous failure of rock structure causing the expulsion of material
RQD:	Rock Quality Designation, empirical measurement of the quality of a rock mass
Seismic Energy:	Form of energy created during a rockburst or earthquake travelling in a waveform
Strain Energy Density:	Rockburst prediction method based on a ratio of the UCS and unloading elastic modulus from a hysteresis loop
Strain Energy Storage Index:	Rockburst prediction method based on a ratio of the strain energy retained and dissipated from a hysteresis loop
Strain Gauge:	Instrument used to measure strain in a rock sample by changing electrical resistances
UCS:	Uniaxial compressive strength
USBM:	United States Bureau of Mines

Rock Type Descriptions

Code	Geological Description
PK	Pyroclastic kimberlite
PKX	Olivine & macrocryst-rich pyroclastic kimberlite
MK	Magnetic lapilli rich macrocrystic volcaniclastic kimberlite
BMVK	Black macrocrystic volcaniclastic kimberlite
MRK	Mud-rich volcaniclastic kimberlite
HK	Coherent kimberlite
VBMK	Variably bedded, mixed mud/macrocryst rich kimberlite

1 Introduction

The objective of this study is to better understand the rockbursting properties of kimberlite. Kimberlite is an igneous rock with diverse properties and composition, occasionally containing diamonds. A rockburst is a natural phenomenon where an abrupt and immediate release of the stored strain energy in a rockmass results in the expulsion of material from the rock face. These seismic events can be very damaging to equipment and underground developments, but more importantly fatal to the miners. The importance of studying and understanding the causes of rockbursts has been emphasized over the last century of recorded incidences. Past research into the causes of rockbursts has proved very successful in the reduction of fatalities from these events.

Previous research is rather extensive; early studies focused on using the properties of the rocks to provide a qualitative determination of a rock's propensity for rockbursting. These methods rely on the UCS, tensile strength, and strain energies from hysteresis loops. Other research focused on gaining insight on the mechanisms which cause rockbursts. The study was based on the idea of an energy balance to account for the sources and destinations for the strain energy. Findings from this research helped in the formation of methods for mitigating the risks of rockbursts. Other systems, have been developed that monitor seismic activity to predict the time and location of potential bursts. These systems have helped to reduce the hazard, but are still not infallible.

The research into the factors that cause rockbursts has proven valuable, but there is still information lacking on distinct rock types. Consequently, little is known of the rockbursting properties of kimberlite, a major diamond bearing rock in Canada's North. Increased underground development in Canada's kimberlite deposits have created interest in better understanding kimberlite's tendency for bursting. The scope of this research focused on assessing the physical properties of kimberlite to determine the rock's bursting propensity. To determine these physical properties uniaxial compressive strength tests, Brazilian tensile strength tests, and cyclic loading tests were utilized.

2 Rockburst Literature Review

2.1 History

Rockbursts have been a hazard to miners since the introduction of underground mining. A rockbursts can occur in both hard rock and soft rock mines; in coal mines bursts can also be referred to as bumps. In Canada, bursts have been prevalent throughout the Sudbury and Kirkland mining regions of Ontario, as well as many other underground mines (Blake & Hedley, 2003). Many of these mines have documented the occurrences of rockbursts over many decades, which aided in understanding the mechanisms that cause them. Figure 2.1 shows a map of historical rockburst prone locations throughout the world. Understanding the rockburst phenomenon is very important; when a burst occurs it can damage mine workings, mining equipment, and injure or kill miners.

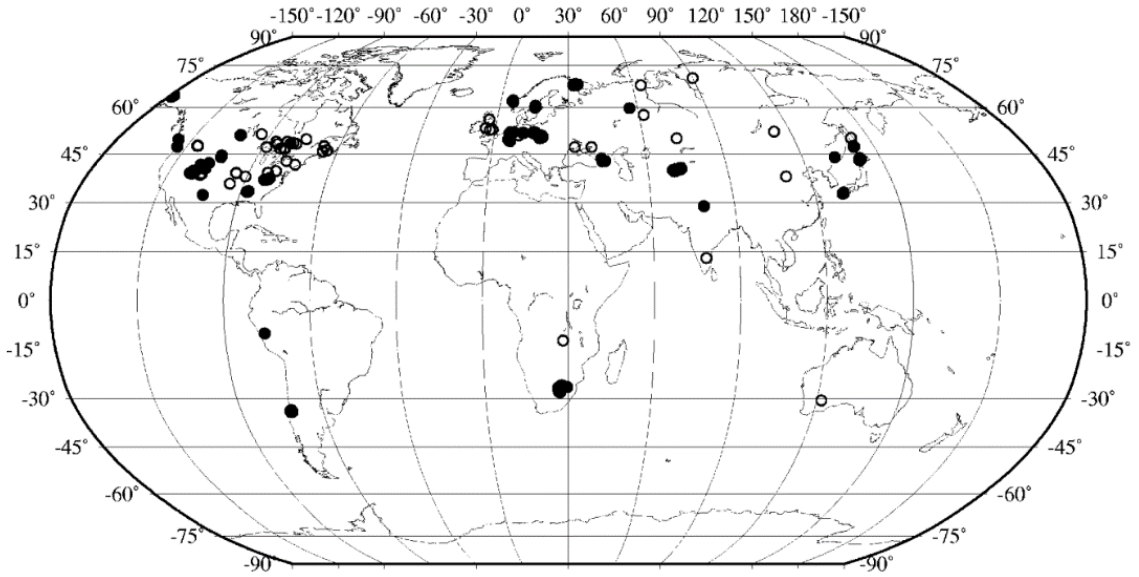

Figure 2.1: Historical rockburst map (Bennett & Marshall, 2001)

2.2 Defining Rockbursts

The phenomenon of rockbursting has several definitions as the causes, scales, and resulting impacts vary greatly from burst to burst. The Ontario Ministry of Labour defines a rockburst as "an instantaneous failure of rock causing an expulsion of material at the surface of an opening or a seismic disturbance to a surface or

underground mine" (Blake & Hedley, 2003). This definition is an attempt to describe the general sense of what a rockburst is and how to identify when one occurs; there are classification systems which label rockbursts depending upon the volume of rock, amount of damage, the vibration duration, and vibration strength (Blake & Hedley, 2003). The violent and sudden nature of a rockburst is its defining characteristics. A seismic event is not necessarily a rockburst, but all rockbursts are seismic events (Hedley, 1992).

During the excavation of an underground mine or tunnel, the induced stresses and energy increase in the remaining rock mass. Rockbursts could be initiated by the unstable release of the energy caused by these mine induced stresses. Another reason why rockbursts occur may possibly be that the mining activities initiate seismic events pre-existing from the geological stresses. Either explanation as to why a rockburst occurs might be correct depending on the circumstances (Cook, 1983).

2.2.1 Classifications of Rockbursts

Rockbursts can fall into different classifications dependent on the causes, size, and impacts. Typically a recorded rockburst is either described as a large seismic event or a small seismic event. A large seismic event can be detected from a distance of 1000 km or greater and can be accompanied by airblasts and seismic waves which damage the underground workings. The airblasts are caused by the large volume of rock which is displaced during the event. Detection of small to medium seismic events is limited to about 100 km from the source. These small events are generally just spalling or popping of the rock and less than 0.5 m^3 of material displaces. Small seismic events do not cause airblasts but short lived seismic waves are generated. A seismic event that is slightly larger at 1 to 2 m^3 is labelled as a bump or knock; sometimes the term rockbump can be used in place of rockburst for these circumstances (Blake & Hedley, 2003).

2.2.2 Types of Rockbursts

There are three categories of rockbursts: strain, pillar, and fault-slip bursts.

The strain bursts occur at the edge of mine openings when stresses are highly concentrated. This kind of burst often happens in development drifts and shafts, particularly when the drift crosses the contact of a brittle and soft rock. The damage from a strain burst can range from the expulsion of rock shards from the wall, to the failure of the entire structure. If the burst is located in a contact between a brittle and a soft rock, the burst will occur in the brittle rock due to its sudden violent failure pattern; whereas the soft rock fails gradually. The stored energy is partially discharged as seismic energy from the rock mass's elastic response (Hedley, 1992).

Pillars are an important part of mine support structures; the failure of a pillar can cause the movement of thousands of tonnes of material. When a pillar burst occurs in one pillar it can cause a chain reaction of pillar bursts as the surrounding pillars become overstressed. When a failure occurs, all of the stored potential energy is released with a large portion becoming seismic energy. Naturally, pillar failures are more susceptible in mining conditions with higher extraction ratios (thus higher stresses), but it is also highly dependent on the geology and natural stress states (Blake & Hedley, 2003).

Fault-slip bursts operate under the same mechanisms as earthquakes. The burst occurs when the frictional resistance created by the normal force is less than the shear stress acting along the fault or other geological structure. This type of burst usually occurs in mines with extensively mined out stopes or areas (>1 km^2) since these large open spaces often expose large geological structures. The magnitude of fault-bursts can be very large and can occur at any time; the way stresses are transferred and the mine geometry are connected to the causes of these bursts (Blake & Hedley, 2003).

2.3 Mining Impacts

The impact which rockbursts have on the operations of a mine varies depending on the size and strength of the burst. Small bursts may only cause damage to equipment and injure personnel, but larger bursts can also cause serious damage to the mine workings requiring considerable rehabilitation. The work to reopen these areas for production cost the mine in both money and time. Controlling when a rockburst occurs is very important and considerable research has been done to create methods for doing so. Figure 2.2 shows the number of reported rockbursts and the resulting fatalities in Ontario mines over the last century. As the graph shows, the work done to control bursting has caused a sharp decline in both rockburst frequency and related deaths over time.

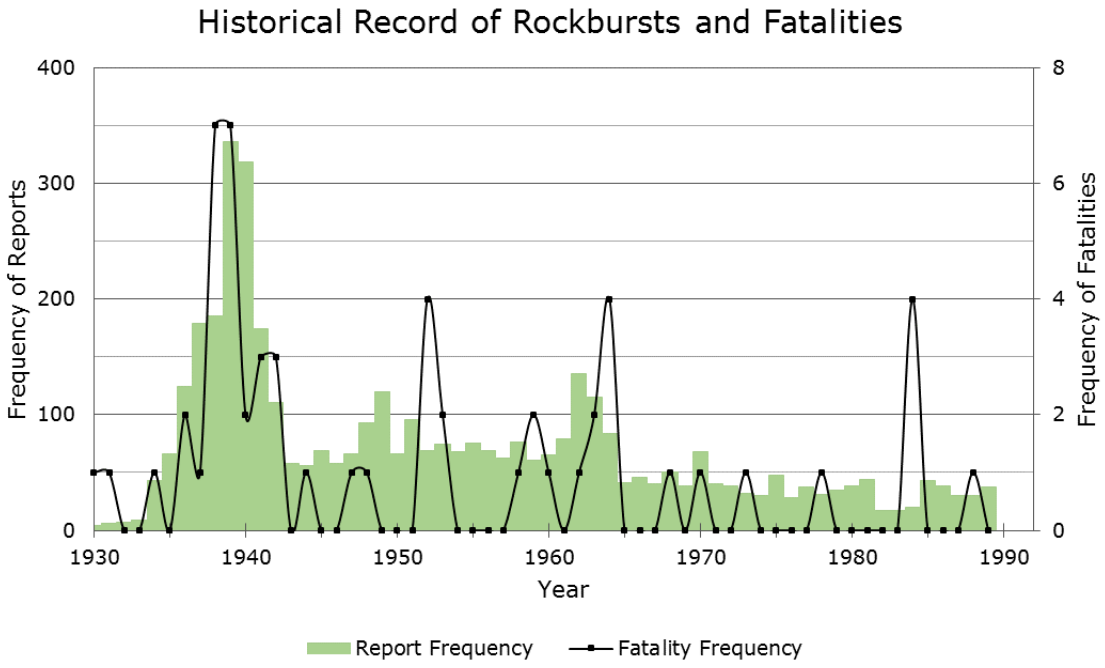

Figure 2.2: Rockburst frequency and fatalities in Ontario Mines (adapted from Hedley, 1992)

2.4 Triggering Mechanisms

There are several mining activities that can trigger rockbursts to occur. Blasting is a major cause of most mining induced rockbursts; the trigger of the burst is not the vibrations but the redistribution of the stresses from the face advance. Drilling underground can also trigger rockbursts; these events are usually much smaller bursts and bumps, but can also cause major pillar bursts. Another trigger is the mucking of ore from the stopes, caused by the removal of support increasing loads on the surrounding pillars (Hedley, 1992).

There are also non-mining related triggers which cause rockbursts. One trigger is that a rockburst can initiate other bursts as stresses are redistributed. Studies have also shown that the weather and rockbursts are strongly correlated. For example, during spring runoffs, it was found that seismic activity increased (Hedley, 1992).

2.5 Mechanics of Rockbursts

As previously described, a rockburst is a sudden and violent release of energy, thus it is possible to describe the mechanics of rockbursts by evaluating the energy in the system. In 1967, Cook developed the concept of energy balance in his work entitled "Design of underground excavations" in the 8th US Rock Mechanics Symposium. Cook's energy balance concept was further developed by Salamon in 1984.

2.5.1 Energy Balance

The general theory behind using energy balance is to understand where the energy is dissipated when rock is excavated. Creating an excavation underground results in a redistribution of the stresses, strains and potential energy in the remaining rock mass; the energy balance that exists is described by equation 2.1. The energy balance equation assumes elastic behaviour in the rock and that fracturing and plastic deformation does not consume energy (Hedley, 1992).

$$W_t + U_m = U_c + W_s + W_r \qquad 2.1$$

$W_t = work\ done\ by\ external\ and\ body\ forces$
$U_m = stored\ strain\ energy\ in\ removed\ rock$
$U_c = strain\ energy\ change\ in\ surrounding\ rock$
$W_s = energy\ disspated\ deforming\ support\ or\ backfill$
$W_r = excess\ energy\ or\ released\ energy$

Salamon describes that there is always excess energy requiring dissipation related with each mining step. The excess energy or released energy (W_r) from equation 2.1 can be seen as the summation of the stored strain energy in the removed rock (U_m) and the seismic energy dissipated during the excavation (W_k) as described by equation 2.2 (Salamon, 1984).

$$W_r = U_m + W_k \qquad 2.2$$

Microseismic systems in mines can measure the seismic energy W_k. The seismic energy component represents the energy from rockburst damage. Replacing W_r in equation 2.1 with equation 2.2 and rearranging for W_k resulting in equation 2.3. Using equation 2.3, the rockburst energy can be calculated, and the strength of the burst that can be expected; assuming that the rock mass is extracted instantly (Salamon, 1984).

$$W_k = W_t - (U_c + W_s) \geq 0 \qquad 2.3$$

Therefore, if it is possible to limit the dissipated seismic energy and released energy (W_r) from mining, it will limit rockburst damage. It is logical to assume that the volume of a mining step is directly correlated to the stored strain energy in a rock, U_m. Therefore, by normalizing the other energy terms by U_m, a comparison can be made to determine the impact of varying excavation volumes. Figure 2.3 shows how the normalized energies are impacted by varying the volume extracted. In the figure a/c represents the ratio of radius increase from a to c of a circular tunnel. Analyzing Figure 2.3, it is evident that when the expansion is small and the ratio a/c is close to 1, the released energy (W_r) is equal to the strain energy of the removed rock (U_m). Based on equation 2.2, the seismic energy dissipated (W_k) must be equal to 0, thus no rockburst

occurs. Therefore, theoretically all of the energy released from mining could be removed with the extracted rock, if the mining step is very small (Salamon, 1984).

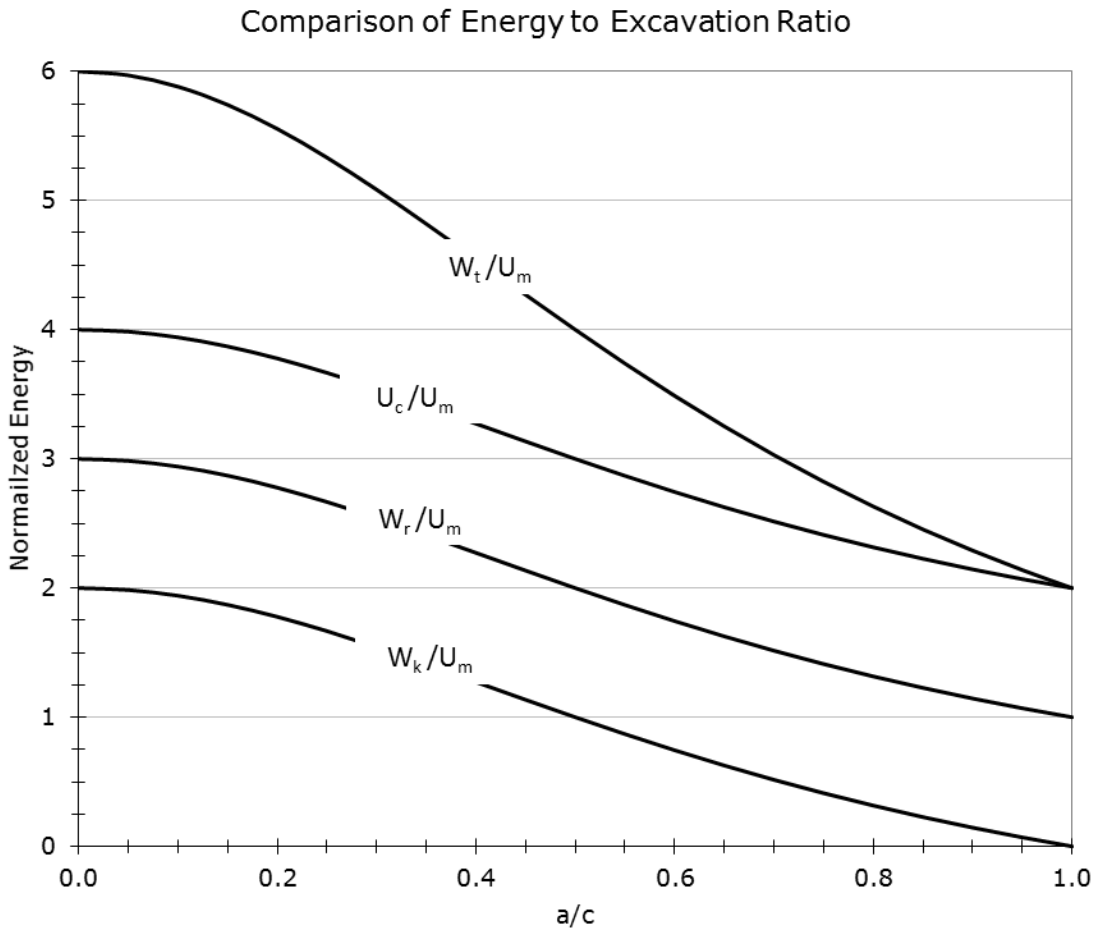

Figure 2.3: Comparison of varying excavation volumes to normalized energies (adapted from Salamon, 1984)

2.6 Prediction Methods Based on Observational Data

2.6.1 Seismic Monitoring

The monitoring of seismic activity around a mine site gives insight into the size and location of rockbursts. Seismic information is collected using three different techniques: seismographs, macro-seismic, and micro-seismic. Seismograph systems are mostly used for large event (earthquake) detection and are positioned on the surface several kilometers from a mine operated by government run organizations (USGS). The macro-seismic system is used to record the waveform of the seismic event and determine its source parameters. The equipment can be located on surface or underground within a kilometer radius of mine workings. Micro-seismic systems monitor the seismic on large and small scales around a mine using geophones and software to triangulate the events location. These systems are operated by the mine and are very sensitive, often mining activity (blasting) triggers a warning (Hedley, 1992).

By collecting seismic information, a mine can generate a map of regions more prone to bursting; maps would aid in the prediction of future burst locations. Furthermore, these maps may even be able to determine which rock types are more likely to cause bursts.

2.6.2 Stress Concentration

Observational data collected from mines in India and South Africa showed that small pillars caused rockburst more frequently than more substantial pillars. It was also noticed that geological discontinuities caused more rockbursts. These observations developed changes to the design of pillars to avoid creating highly stressed situations. The connection between the concentration of stresses and rockbursts was established and resulted in attempts to quantitative estimates of the stresses in a mine to predict the location of potential bursts. Today, the development of computer models allows for more complex analysis of the mine designs to find areas of high stress concentrations and to adjust the mine design or decide whether to utilize techniques such as distress blasting. These models provide important information but it is limited in that it can only identify areas of concern but cannot predict if a rockburst is actually going to occur (Hedley, 1992).

2.6.3 Micro-Seismic Activity

Interest in micro-seismic prediction of rockbursts was first generated by the USBM. The technology to effectively measure this activity took many years to develop to the point in which the origin location of the seismic event could be accurately determined, through geo-phone arrays and time of arrival information. Using this technology, burst prone structures in mines could be identified and computerizing the system allowed for 24 hour monitoring and analysis. Sometimes the micro-seismic activity will build up in a location prior to a burst allowing for preventative measures to be taken to protect people and equipment. However, bursts have also been shown to occur without any micro-seismic warnings and other times a large amount of activity exists without producing a rockburst. From micro-seismic monitoring experiences, these systems are capable of delineating specific structures in a mine prone to bursting but reliable predictions of rockbursts require more information (Hedley, 1992).

2.6.4 Time of Burst Prediction

Predicting the location of where a rockburst is going to occur has been quite successful but predicting the time when it will occur has proven to be very difficult. The difficulty in predicting when a burst will occur is due to the lack of understanding of the contributing factors. One method is to analyze the distribution rockburst frequency to determine where in the mining cycle most bursts occur. A study found that most bursts occurred during or quickly after blasting at some mines, while contrary data was found at other mines (Hedley, 1992). Some mines utilized microseismic geophones to measure the seismic activity, which were useful for determining areas that are burst prone. Improvements in microseismic monitoring has made it a useful tool in modern mines for daily monitoring, reducing rockbursting risks while increasing safety and productivity. (Ge, 2005)

2.7 Prediction Methods Based on Rock Properties

2.7.1 Strain Energy Index Method

The Strain Energy Storage Index is a simple and useful method for the prediction of rockburst propensity in rocks. The Strain Energy Storage Index (W_{ET}), is calculated by comparing the amount of elastic strain energy stored and the elastic strain energy that is dissipated during a loading and unloading cycle on a rock specimen. The elastic hysteresis loop is developed by loading a sample to 80-90% of the UCS and then completely releasing the applied load at the same stress rate. The Strain Energy Storage Index is calculated as shown by equation 2.4. Studying coal samples, Kidybinski found that a $W_{ET} < 2$ produced brittle fragmentation, a $2 \leq W_{ET} < 5$ produced transitional failure characteristics, and $W_{ET} \geq 5$ produced violent failures (Kidybinski, 1981).

$$W_{ET} = \frac{\phi_{sp}}{\phi_{st}} \qquad 2.4$$

$$\phi_{sp} = strain\ engergy\ retained$$

$$\phi_{st} = strain\ energy\ dissipated$$

The strain energy retained and the strain energy dissipated by the rock sample are calculated with the elastic hysteresis loop. The area under the unloading curve represents the retained strain energy and the area between the loading and unloading curves represent the strain energy that was dissipated; Figure 2.4 graphically defines the retained and dissipated energy areas. The dissipated energy is due to the formation of micro-fractures in the rock as it is loaded, releasing the stored potential energy (Wang & Park, 2001). Based on the equation for W_{ET}, the larger the retained energy and the smaller the dissipated energy; the more violent and sudden the failure of the rock is likely to produce.

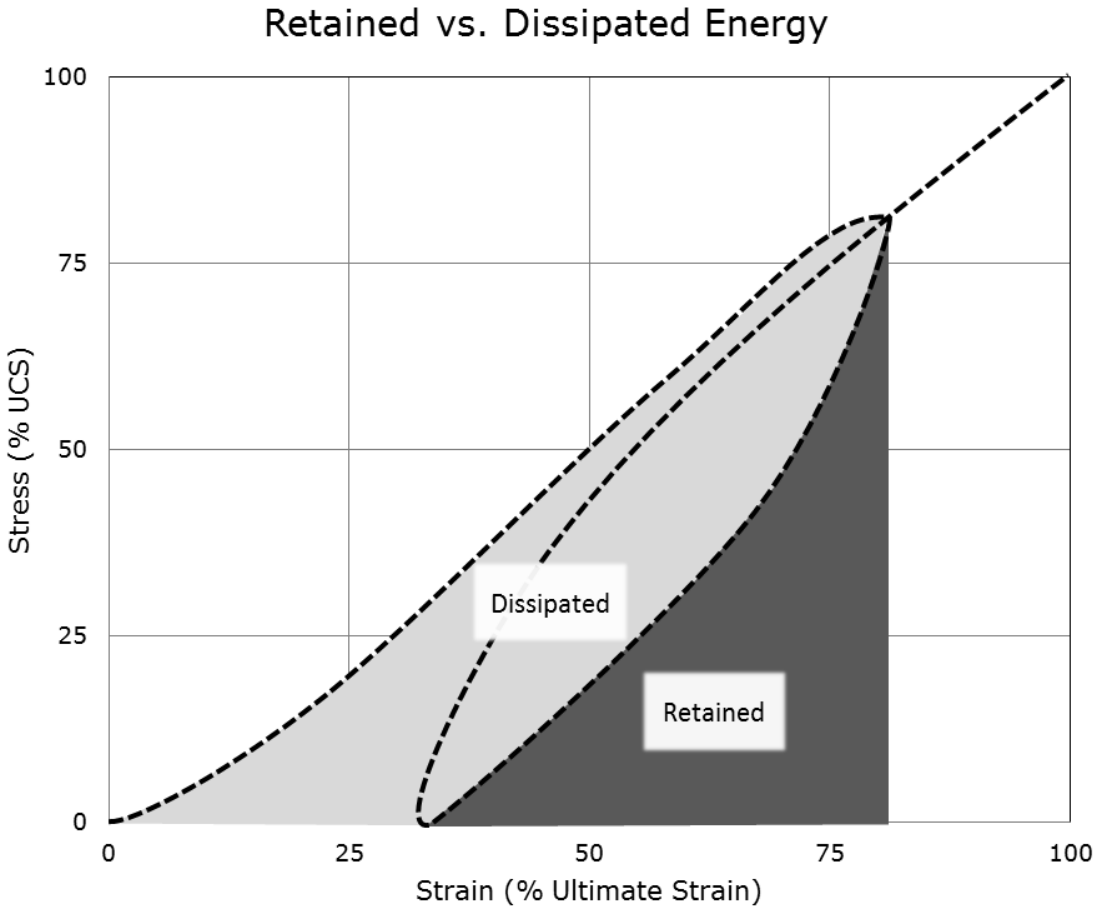

Figure 2.4: Stress-strain graph showing dissipated and retained energy from hysteresis loop (adapted from Wattimena, Sirait, Widodo, & Matsui, 2012)

2.7.2 Strain Energy Density Method

Kidybinski developed the indices to determine the probability of rockbursting using coal, which does not allow for plastic deformation, unlike harder, more competent rock types. To predict the rockbursting propensity of hard rocks the Strain Energy Density (SED) theory is utilized. To calculate the SED, equation 2.5 is used making the assumption that the specimen is linearly elastic (Wattimena, Sirait, Widodo, & Matsui, 2012). Figure 2.5 indicates where the unloading elastic modulus is calculated from on the hysteresis loop.

$$SED = \frac{\sigma_c^2}{2E_s} \qquad 2.5$$

$$\sigma_c = UCS\ (MPa)$$

$$E_S = unloading\ elastic\ modulus\ (MPa)$$

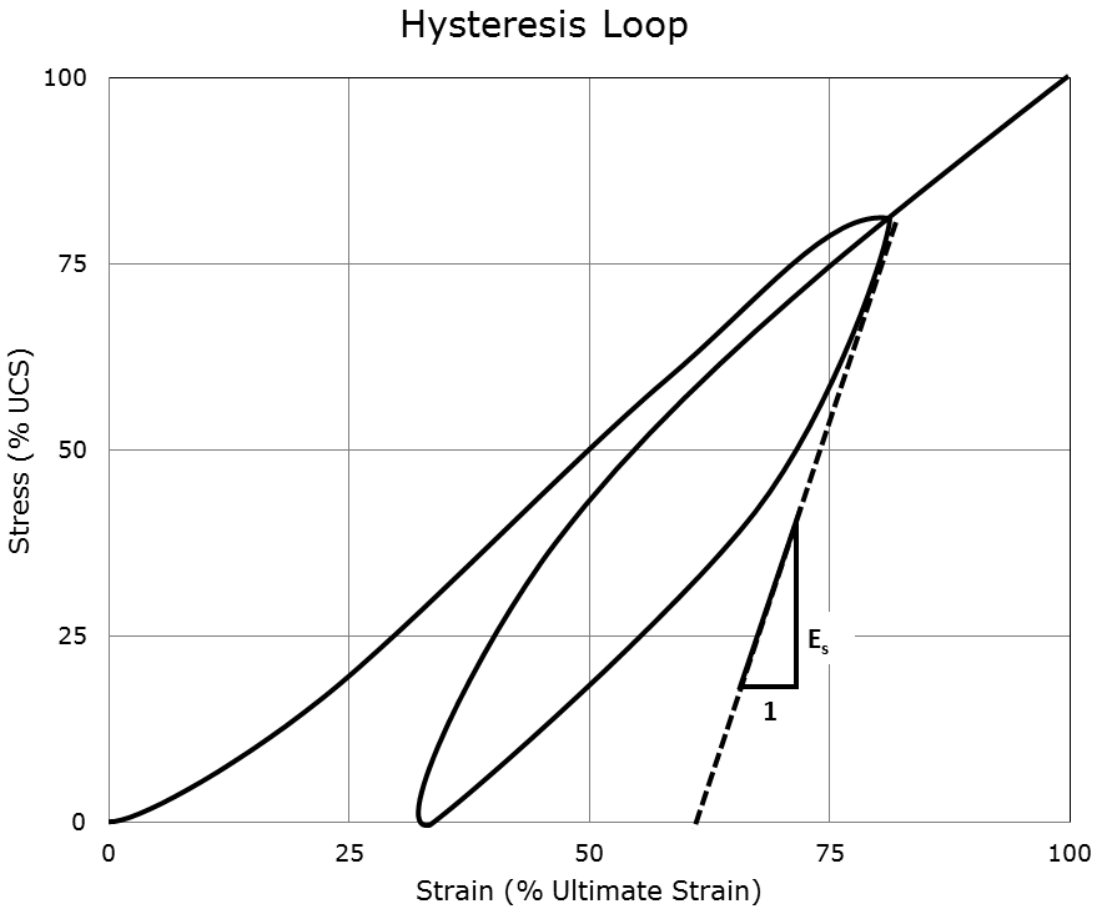

Figure 2.5: SED hysteresis loop indicating the unloading elastic modulus (adapted from Wang & Park, 2001)

Using the relationship described and Table 2.1, the relative probability of rockbursts occurring can be estimated. The rating system is qualitative and thus can only provide an idea if rockbursting is a problem that should be mitigated and further insitu testing carried out.

Strain Energy Density (kJ/m^3)	Hazard Potential
SED ≤ 50	Very Low
50 < SED ≤ 100	Low
100 < SED ≤ 150	Moderate
150 < SED ≤ 200	High
SED > 200	Very High

Table 2.1: SED rockburst hazard rating system (Wattimena, Sirait, Widodo, & Matsui, 2012)

2.7.3 Rock Brittleness Method

It has also been shown experimentally that the brittleness of a rock can be related to the strength of rockbursts. The brittleness of a rock is calculated as shown in equation 2.6. Based on the brittleness of the rock and using Table 2.2 it is possible to estimate the relative strength of the rockburst potentially produced. Similar to the Strain Energy Index method the rock brittleness does not give quantitative measures of the rockburst strength but rather a qualitative estimates of the rockburst strength (Wang & Park, 2001).

$$B = \frac{\sigma_c}{\sigma_T} \qquad 2.6$$

$$\sigma_T = \ tensile\ strength\ (MPa)$$

$$\sigma_c = \ UCS\ (MPa)$$

Brittleness Value	Rockburst Strength
B > 40	No Rockburst
26.7 < B ≤ 40	Weak
14.5 < B ≤ 26.7	Strong
B > 14.5	Violent

Table 2.2: Rockburst strength estimation based on rock brittleness (Wang & Park, 2001)

2.7.4 Tangential Stress Method

Another method to determine the strength of a possible rockburst is to use insitu stress measurements from the rockmass and the rock's uniaxial compressive strength. The calculation of the tangential stress is made using equation 2.7.

$$T_S = \frac{\sigma_\theta}{\sigma_c} \qquad 2.7$$

$\sigma_\theta = \ tangential\ stress\ (MPa)$

$\sigma_c = \ UCS\ (MPa)$

The tangential stress is measured in the rockmass around the stope or underground workings. The measurements can either be made in place or done through a numerical model. Based on the ratio of the tangential stress and the uniaxial compressive strength the strength of the rockburst can be estimated using the guidelines in Table 2.3. Of the four indices discussed, only the tangential stress takes into account stress regime of the rock being analyzed.

Tangential Stress	Rockburst Strength
$T_S < 0.3$	No Rockburst
$0.3 \leq T_S < 0.5$	Weak
$0.5 \leq T_S < 0.7$	Strong
$T_S \geq 0.7$	Violent

Table 2.3: Rockburst strength estimation based on the tangential stress (Wang & Park, 2001)

2.7.5 Classification using RQD Index Method

Logically, the more fractured a rockmass is the smaller the probability for rockbursts to occur because the stresses that build up are able to be transferred further away from the excavation. If the rockmass is less jointed and more massive the stresses can accumulate and focus increasing the likelihood of bursting. Therefore, it is a reasonable assumption to make the connection between the Rock Quality Designation (RQD) and the rockbursting propensity of a rock type (Wang & Park, 2001). To apply this in a mining situation it would be necessary to make a custom rating system based on the known rockbursts compared to the RQD index of that rock type in that particular area. Then it would be possible to make reasonable estimates of future rockburst prone locations.

3 Case Study

3.1 Diavik Diamond Mine Background

The Diavik Diamond mine operates in the Northwest Territories on an island in Lac Des Gras located 300 km North East of Yellowknife. The mine opened in 2003 starting as an open pit operation producing diamonds from three kimberlite pipes; A154N, A154S, and A418. The mining of the pipes can be seen in Figure 3.1. Starting in 2012 the mine transitioned over to an underground operation to continue extraction of diamonds and will continue production until 2023 (Diavik Diamond Mine, 2012).

Figure 3.1: Aerial view of the Diavik Diamond Mine (Rio Tinto, 2015)

3.1.1 Underground Mining Methods

The A418 and the A154S pipes utilize a caving method called sub-level retreat or SLR (Diavik Diamond Mine, 2012). The mining proceeds from the top of the ore body to the bottom with subsequent levels being made to drill, blast, and remove the broken ore. This method relies on gravity to draw the ore to draw points, which is then moved to the surface by equipment. The mining method used in A154N is called blasthole

stoping (Diavik Diamond Mine, 2012). This method proceeds from bottom to top and involves drilling vertically between two drifts and then blasting off slices of the stope. The opening is then backfilled with a cemented rock to stabilize the opening facilitating the mining of the adjacent stopes. The main difference between the two methods is that blasthole stoping employs a crown pillar made of ore. The crown pillar is often difficult to completely recover and can result in millions of dollars of potential profit being left in place. The mining development underground can be seen in Figure 3.2. The underground working that have been excavated are shown in grey and future development is shown in blue and green. As the drawing illustrates, the mine still has a fairly large amount of development and mining until the remainder of the kimberlite pipes have been completely extracted.

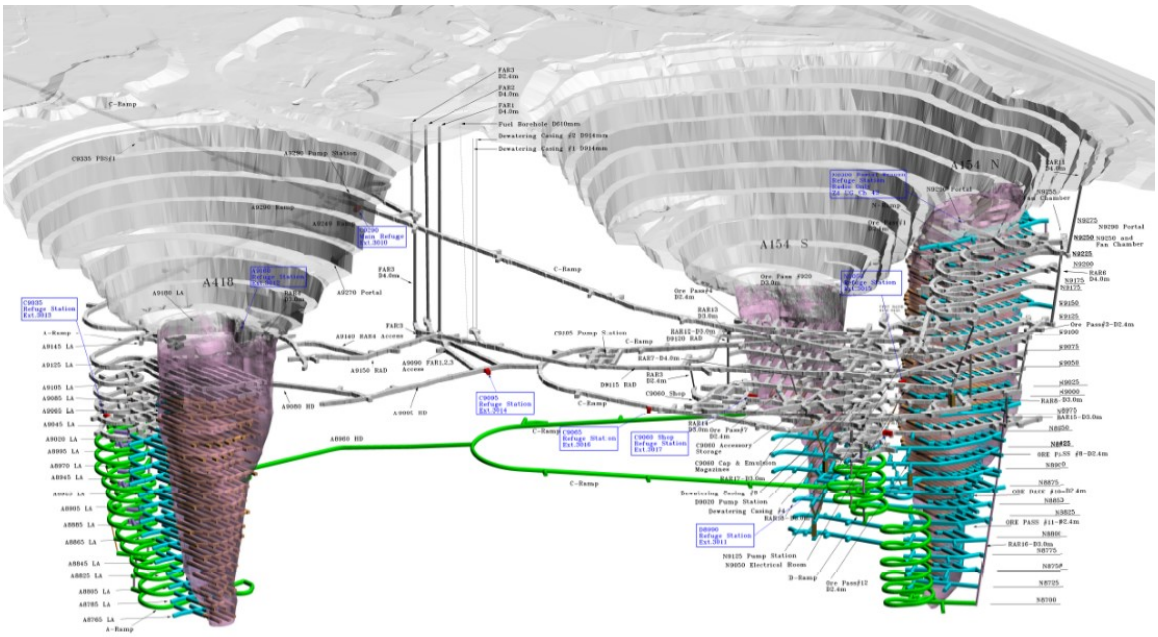

Figure 3.2: Underground development at the Diavik Diamond Mine (Rowmanowski, 2014)

3.1.2 Geology of Kimberlite

Kimberlite is an igneous ultramafic rock of volcanic origins; often it is found as diatremes, dikes, or sills. A relatively rare rock, it is typically fine to medium grained with a unique gray green/blue colour. From a chemical standpoint, kimberlite is distinguishable with a high magnesia, very low silicon dioxide, and high titanium dioxide contents. (Magill, 1990)

The formation of the kimberlite deposits is not fully understood but most believe that the rock originates from a great depth (up to 600 km) below the earth's surface; it is then brought to the surface through networks of fractures in the earth's crust in an explosive nature. Because of the explosiveness and path which the kimberlite forming material takes, it often gathers xenoliths and crystals. The mixing of the kimberlite forming material and the fragments of other rocks and crystals makes kimberlite a very complex rock with properties unique to each deposit. (Magill, 1990)

The grain sizes of kimberlite varies considerably due to the xenoliths and megacrysts found in the fine grained matrix. The common megacrysts found in kimberlites are olivine, mica, pyroxene, and garnets. Occasionally kimberlites will also contain diamonds, which represent the main value in the rock, although the diamonds are not always gem quality. (Magill, 1990)

3.1.3 Rock Types at Diavik

There are two main rock types faced in the mining of the diamond pipes at Diavik: granite and kimberlite. The diamond pipes are made of the kimberlite surrounded by the considerably older granite, known as the Canadian Shield. The kimberlite is further categorized into several sub rock types. The difference between the rock types is based on the grain sizes, matrix constituents, geological properties, and the method of formation. Kimberlite is known for its high variability and unpredictable nature; which is why, each kimberlite pipe has many sub-rock types differentiated. A 3D map of the rock types can be seen in Figure 3.3 and cross sectional maps in Figure 3.4.

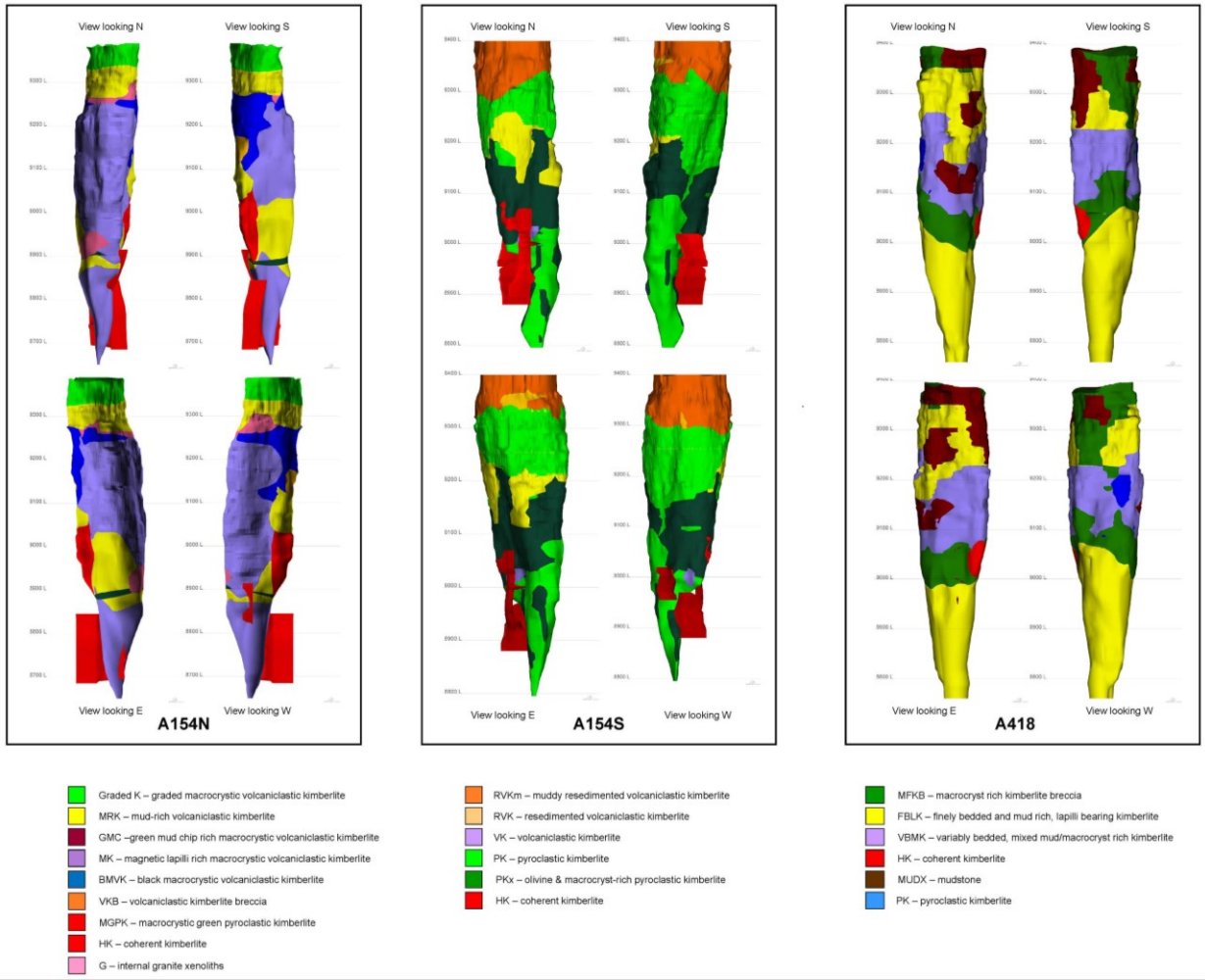

Figure 3.3: 2014 Kimberlite rock type map at Diavik (Rowmanowski, 2014)

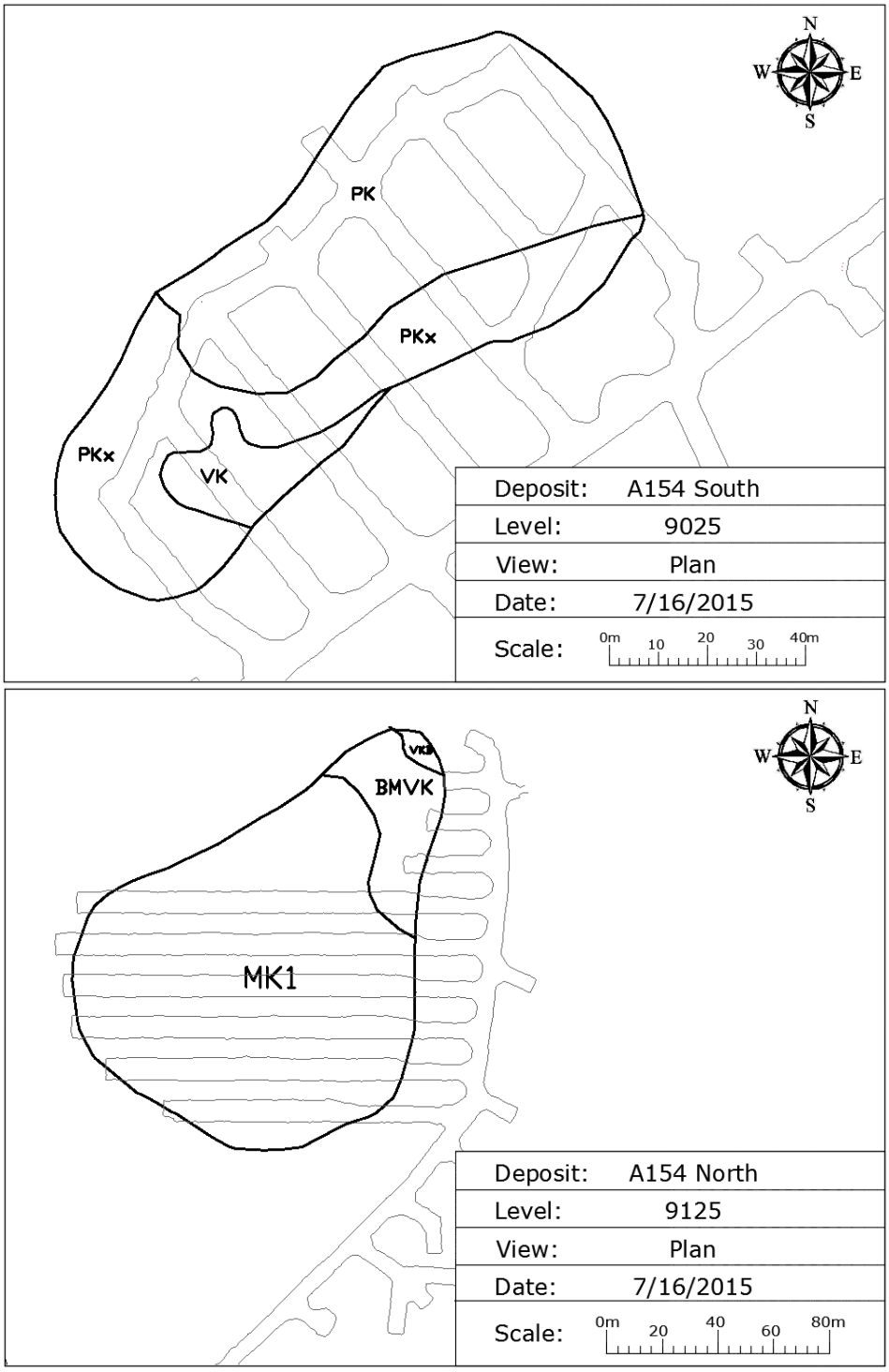

Figure 3.4: Cross sections of the south & north pipes showing the current development and rock types (Rowmanowski, 2014)

The developments in Figure 3.4, indicate the variety of rock types that can be encountered on any one level. Each of these rock types will have unique properties and react differently under the changing stress regimes that are created during the mining process, including rockbursting properties.

The rock type volume percentage breakdowns for each pipe are listed in Table 3.1. As is shown in that table, the pipes are comprised of a great variety of rock types some of which such as HK and RVK are found in both the North and South pipe. The North pipe mostly contains MK and MRK, with the former totalling 54% of the pipe's volume. PK and PKX are the two main rock types found in South pipe together taking up 63% of the volume. A418 is slightly different from the other pipes in that it has three rock types that account for a majority of the volume. The main rock types for A418 are VBMK, FBLK, and MFKB totalling 94% of the pipe.

Deposit	**A418**		**A154 North**		**A154 South**	
Rock Types	FBLK	41%	MK	54%	PK	41%
	VBMK	28%	MRK	22%	PKX	22%
	MFKB	25%	GRADEDK	8%	RVK	15%
	MUDX	4%	GMC	7%	RVKS	12%
	BMCK	1%	BMVK	5%	RVKM	9%
	INTMUDX	0.3%	HK	2%	VK	1%
			RVK	2%	HK	1%
					MUDX	0.1%

Table 3.1: Rock type percent volume breakdown of each pipe (Fomradas, 2015)

3.2 Motivation of Research

Since moving to an underground operation, Diavik has experienced relatively small failures that appear to be rockbursting related. Rockbursting as described earlier is a dangerous phenomenon that can damage equipment and hurt or fatally injure employees. However, through the use of different rock properties and how they relate to rockbursting, it is possible to identify the relative probability and strength of a rock's bursting behaviour. There are several different rock types at Diavik and thus it will be necessary to test each rock type to determine its bursting propensity. The experiments consist of uniaxial compressive strength tests, tensile strength tests (Brazilian tests), and cyclic loading tests to define a hysteresis loop. The results were compared to the suggested ranges given by other researchers. From the results, direction was given as to which types of kimberlite are more likely to create rockbursts. By identifying the burst behaviour of the different rock types, this allows a mining operation to detect areas of concern before mining activity in the rock occurs.

4 Method of Research

Based on the literature review, to determine the rockbursting propensity of a rock, it is necessary to understand its properties and characteristics. The necessary information includes the uniaxial compressive strength, tensile strength, Young's modulus, Poisson's ratio, and hysteresis loop. To determine all of these characteristics three unique experiments will be conducted: tensile strength tests, uniaxial compressive strength tests, and cyclic loading tests. Each experiment was conducted a minimum of three times for each rock type as Diavik Diamond Mine agreed to supply the samples necessary for this quantity of tests. More experiments than the minimum were conducted based on the availability of additional samples.

4.1 Experiment Descriptions

All experiments were carried out following applicable American Standard Testing Methods (ASTM) documentation when possible. In some cases, no ASTM or similar standard testing methods existed. In these situations, the tests were carried out following a procedure developed from literature and the capabilities of the equipment.

4.1.1 Tensile Strength Tests

The tensile strength of the samples will be determined using the Brazilian tensile strength test (also referred to as the splitting tensile strength test). The procedure for the experiment, as well as the preparation of the samples will be taken from ASTM D3967 – 08, the Standard Test Method for Splitting Tensile Strength of Intact Rock Core Specimens. The Rock Mechanics Department at the University of Alberta has a piece of equipment specifically for conducting these experiments and an image of the device is shown in Figure 4.1. This instrument is only capable of accommodating the larger sample size; the smaller 1.5 inch samples were done using loading platens top and bottom which is also an acceptable method of conducting the test. The Brazilian test uses the maximum load recorded in N, sample dimensions, and equation 4.1 to calculate the tensile strength in MPa. The calculation is an estimate of the tensile strength of the rock sample.

$$\sigma_t = \frac{2P}{\pi LD} \qquad 4.1$$

$\sigma_t = Tensile\ Strength\ (MPa)$

$P = Max\ Load\ (N)$

$L = Thickness\ of\ Sample\ (mm)$

$D = Diameter\ of\ Sample\ (mm)$

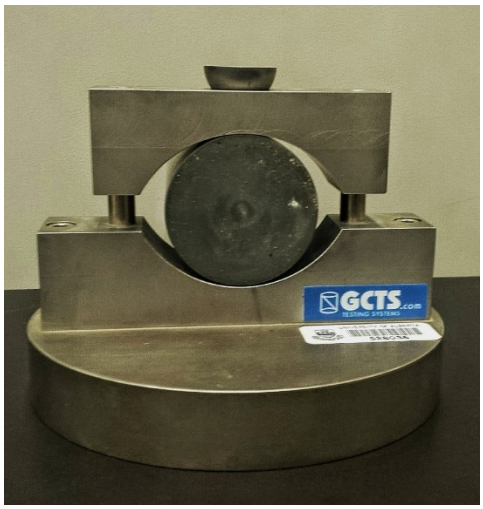

Figure 4.1: Brazilian tensile strength test equipment

4.1.2 Uniaxial Compressive Strength Tests

These experiments will be conducted using two different machines depending on the size of the cores. The larger cores will be tested using the Instron loading frame in the Rock Mechanics Laboratory and the vertical and horizontal deformations will be measured using LVDTs on a compressometer; the compressometer can be seen in Figure 4.2. The other tests were conducted using the MTS loading frame in the Structures laboratory and the deformation measurements were collected by strain gauges. The Instron machine was not able to accept strain gauges and is the reason why the different sample sizes have their respective loading frames. The procedure which was followed is that described by ASTM D7012 – 13, the Standard Test Methods for Compressive Strength and Elastic Moduli of Intact Rock Core Specimens under Varying States of Stress and Temperatures. The results from these experiments will be used to determine the UCS, Young's modulus, and Poisson's ratio of each rock type.

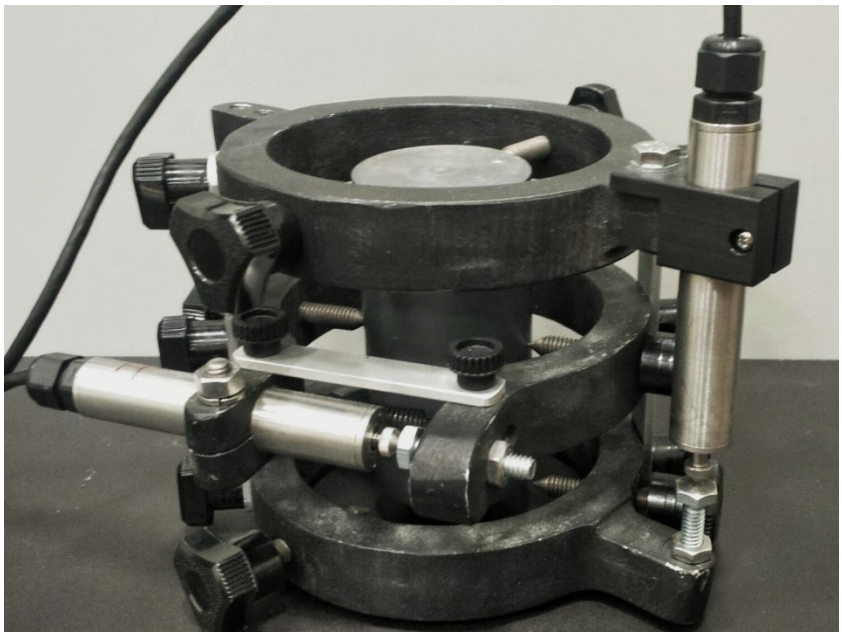

Figure 4.2: Compressometer with LVDT arrangement for vertical and horizontal deformation measurements

4.1.3 Hysteresis Loop Tests

As was done with the UCS tests, the same two loading frames were used for the respective sample sizes. An ASTM or similar standard for cyclic loading tests on rocks could not be found, so to conduct this experiment the ASTM for the UCS tests was used in conjunction with the suggestions made by the literature. The recommendation is to load the sample to 70-90% of its UCS strength and then completely unload and then reload the sample till failure (Kidybinski, 1981). The loading and unloading of the sample was done at the same rate which was 0.5 MPa/s and since the strength of the sample could not be estimated with great accuracy, the loading was done in 25% incremental increases until the failure occurs; a sample pattern is shown in Figure 4.3. The loading pattern was done in such a way to attempt to always get a load/unload cycle between 70-90% UCS of the sample.

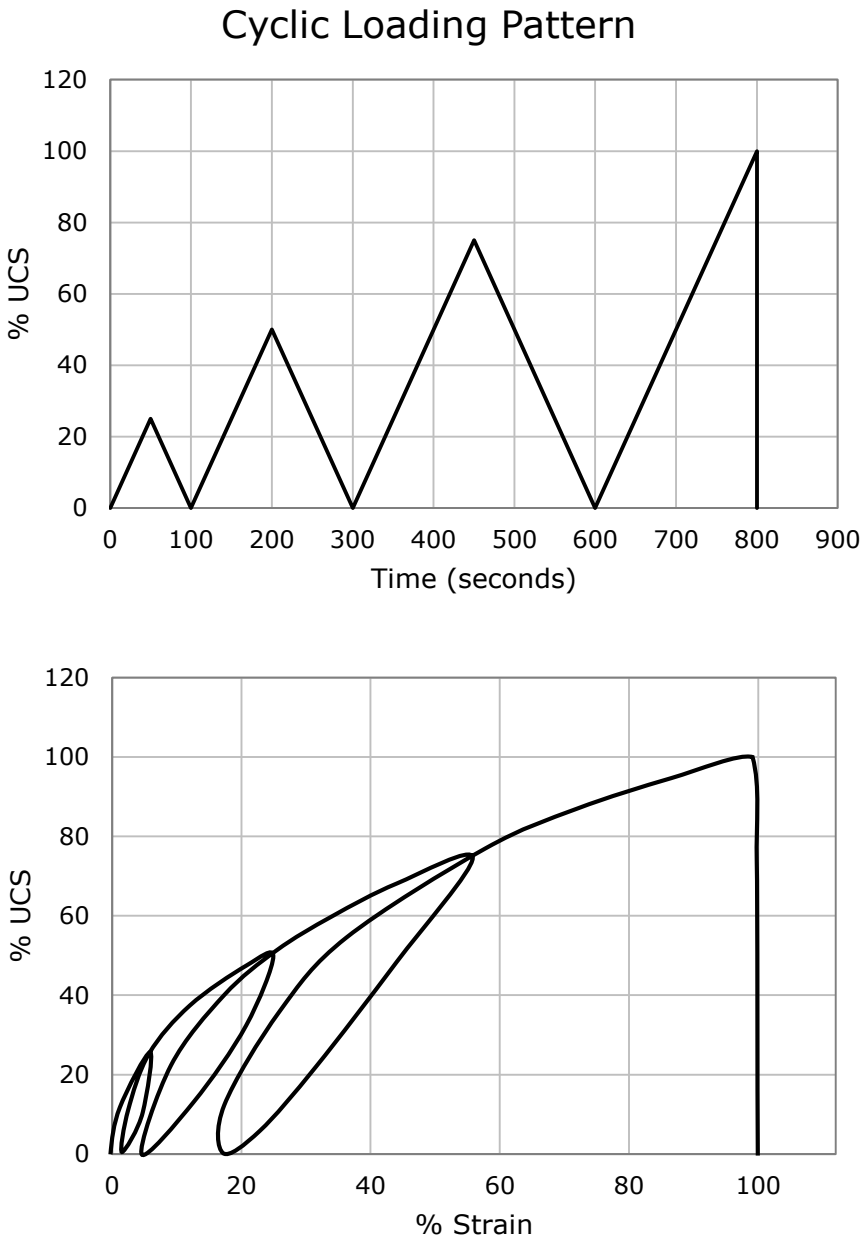

Figure 4.3: Loading Pattern for the Cyclic Loading Tests

4.2 Sample Preparation

The nature of the research method dictates that a large number of samples must be prepared. Diavik was willing to provide kimberlite from seven different rock types. The rock type names are dependent on the geological properties, a list of the rock types supplied and their description are shown below in Table 4.1.

Kimberlite Pipe	Code	Geological Description
A154 South	PK	Pyroclastic kimberlite
	PKX	Olivine & macrocryst-rich pyroclastic kimberlite
A154 North	MK	Magnetic lapilli rich macrocrystic volcaniclastic kimberlite
	BMVK	Black macrocrystic volcaniclastic kimberlite
	MRK	Mud-rich volcaniclastic kimberlite
	HK	Coherent kimberlite
A418	VBMK	Variably bedded, mixed mud/macrocryst rich kimberlite

Table 4.1: Rock codes and geological descriptions

The samples from the mine came in two different varieties: core and bulk sample rocks. The core that was provided was large at 63.5 mm in diameter and the bulk sample rocks varied considerably in size but were typically rectangular prisms. The bulk samples required coring and because of its small size, it was only feasible to produce cores of 38 mm in diameter; the coring is shown in Figure 4.4. Once cored the samples were measured and trimmed to meet the required ASTM ratios as seen in Figure 4.5. The ends of the samples were then sanded to remove irregularities and create parallel faces; a finished product of cored sample can be seen in Figure 4.6. The UCS ASTM requires at least a 2:1 height to diameter ratio and the Brazilian test ASTM requires a thickness to diameter ratio of 0.2 to 0.75. The complete list of samples created and corresponding measurements can be seen in Appendix A.

Figure 4.4: Coring of bulk rocks samples

Figure 4.5: Trimming samples with wet saw

Figure 4.6: Finished sample ready for testing (38mm diameter)

4.2.1 Sample Preparation Difficulties

During the process of creating the samples there were considerable problems encountered. Many samples were eroded during the coring and cutting process to the extent that prevented the creation of any usable sample for the uniaxial compressive strength and hysteresis loop experiments for rock type VBMK. These difficulties could have been due to the grainy and low matrix content of the VBMK rock type. Some changes to the preparation procedure was done to help prevent this erosion issue. A dry saw was used in place of the wet saw for erodible samples. Also, more insitu core samples were sent from the mine in place of rock samples that would need coring. The dry saw and insitu core samples effectively solved the issue.

5 Experimental Results

5.1 Tensile Strength

The Brazilian tensile strength experiments were carried out on the seven rock types and the maximum loads recorded. These loads were then used to calculate the tensile strength in MPa. The calculated results for each rock type can be seen in Figure 5.1 along with the corresponding average. The complete results from all of the Brazilian experiments can be seen in Appendix B including the maximum load, the calculated tensile strength, and the average tensile strength. Analyzing the results shown in Figure 5.1, it is clear that certain rock types display tremendous variability and other rock types show more consistent results.

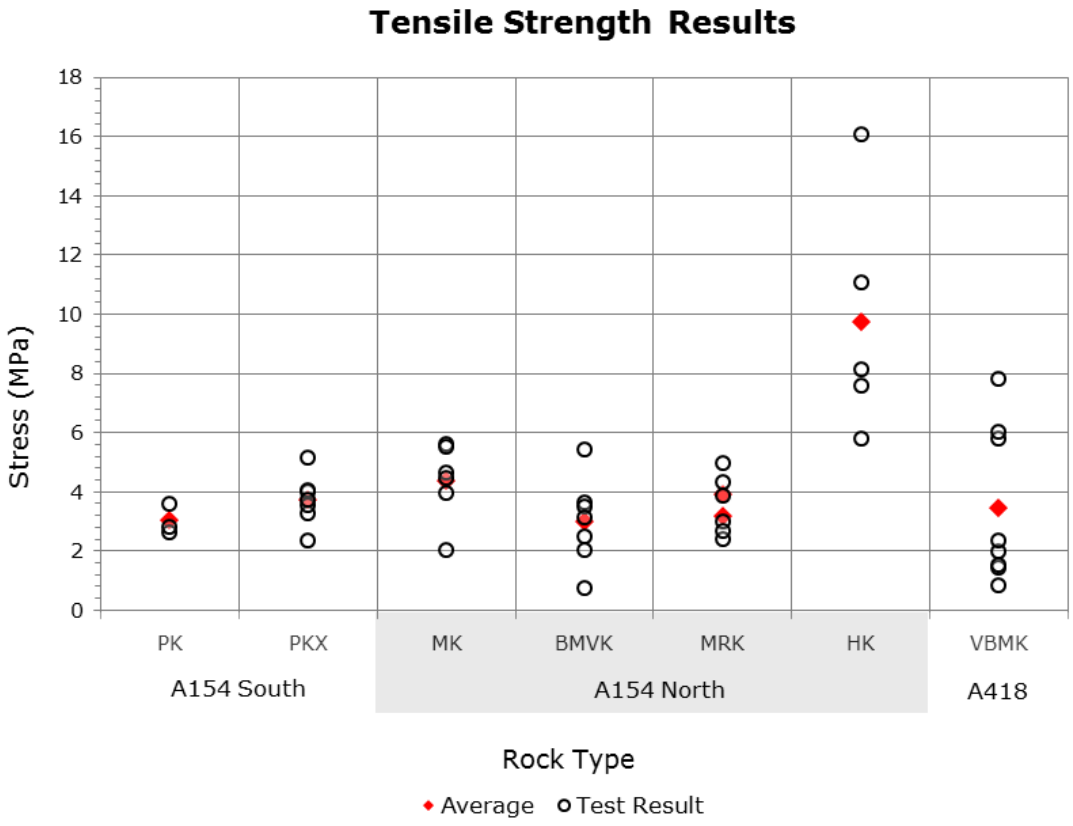

Figure 5.1: Tensile strength results of samples tested

The VBMK and HK rock types for instance showed a considerable range of strengths, whereas MRK and PK were much tighter. The average tensile strength for six of the seven rock types was fairly consistent, falling in the range of 3 to 4.5 MPa. HK was the only rock type that showed a high average tensile strength of 9.7 MPa. The two average points for MRK indicate the difference between the large and small diameter cores results. The average tensile strengths of the MRK cores tested were very similar and indicated that the size of the core did not have a significant impact on the tensile strengths.

The tensile strengths of common rocks compared to the tensile strength of the kimberlite samples is shown in Figure 5.2. Kimberlite being an igneous, is in the weaker region of the range of igneous rocks listed.

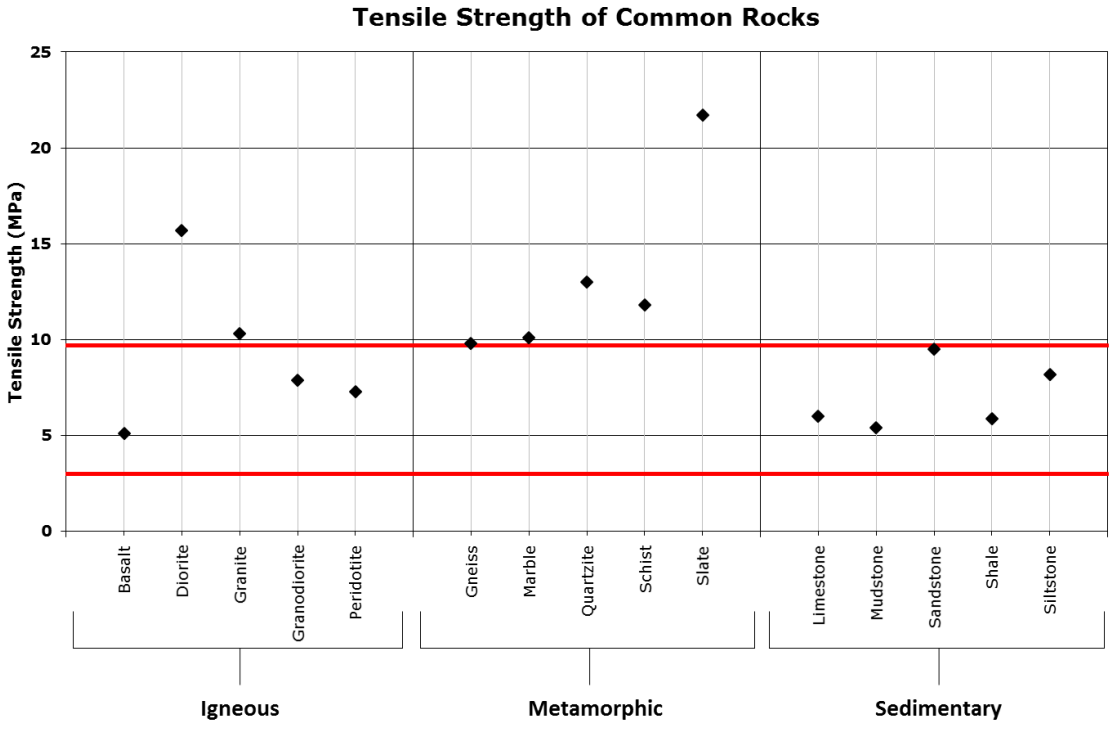

Figure 5.2: Tensile strength of common rocks (adapted from Perras & Diederichs, 2014)

5.2 Uniaxial Compressive Strength

The uniaxial compressive strength experiments were only performed on six of the seven rock types due to sample numbers and difficulties encountered in the coring process for the VBMK rock type. The UCS for each sample was calculated from the maximum load (kN) measured during the experiment and then divided by the cross-sectional area of the sample. The results from the calculations indicate that the UCS of kimberlite is slightly better behaved than the tensile strength, MK and MRK being the exception as seen in Figure 5.3.

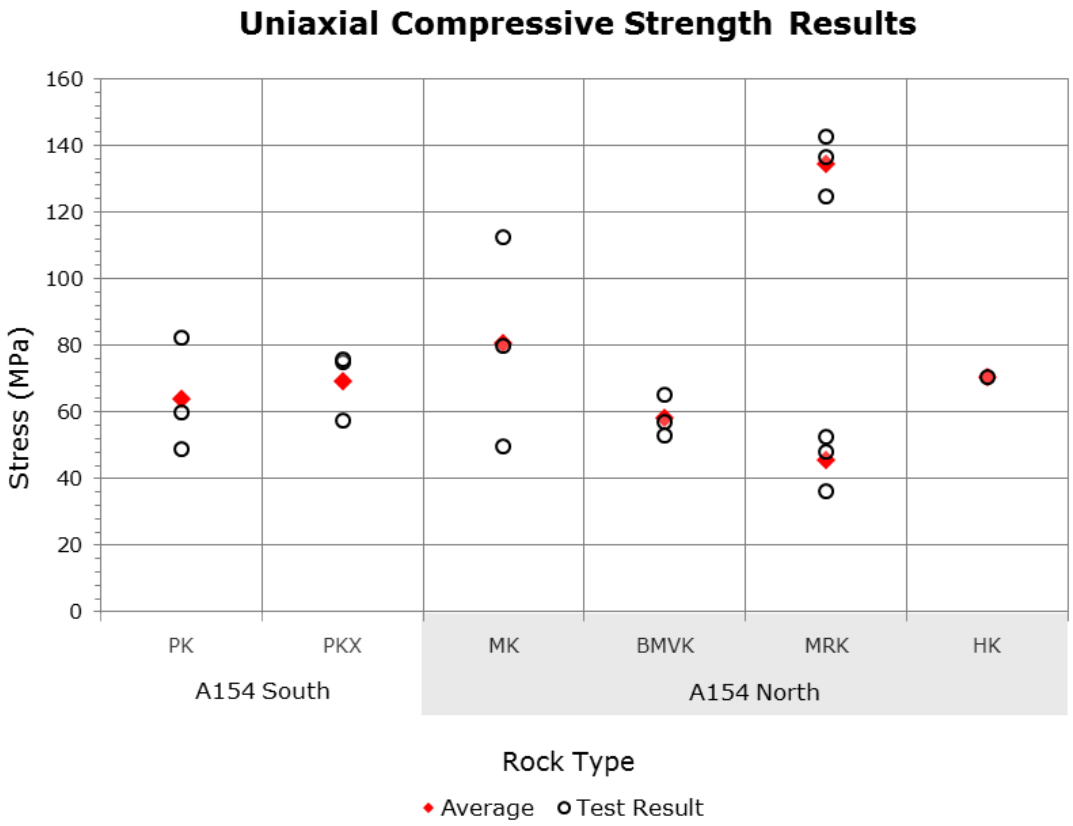

Figure 5.3: Uniaxial compressive strength test results

The UCS of MK ranged substantially from 50 to 113 MPa; the source of the differences could be due to sample preparation, mistaking rock types during sampling, and natural variability. Another surprising result was the strength of the MRK rock type, which averaged a UCS of 135 MPa. The strength of MRK was very surprising given that kimberlite is known as a weaker rock and a strength of 135 MPa is fairly strong. Because of these results more testing was done on MRK using larger diameter cores. The second set of testing on MRK produced considerably lower UCS values with an average of 46 MPa. It is more likely that the strength of MRK is closer to the lower average since larger cores are more representative of the rockmass. The HK rock type provided had only a single specimen fitting the testing parameters. The UCS strength of HK was similar to that of the other rock types other than the smaller MRK core results.

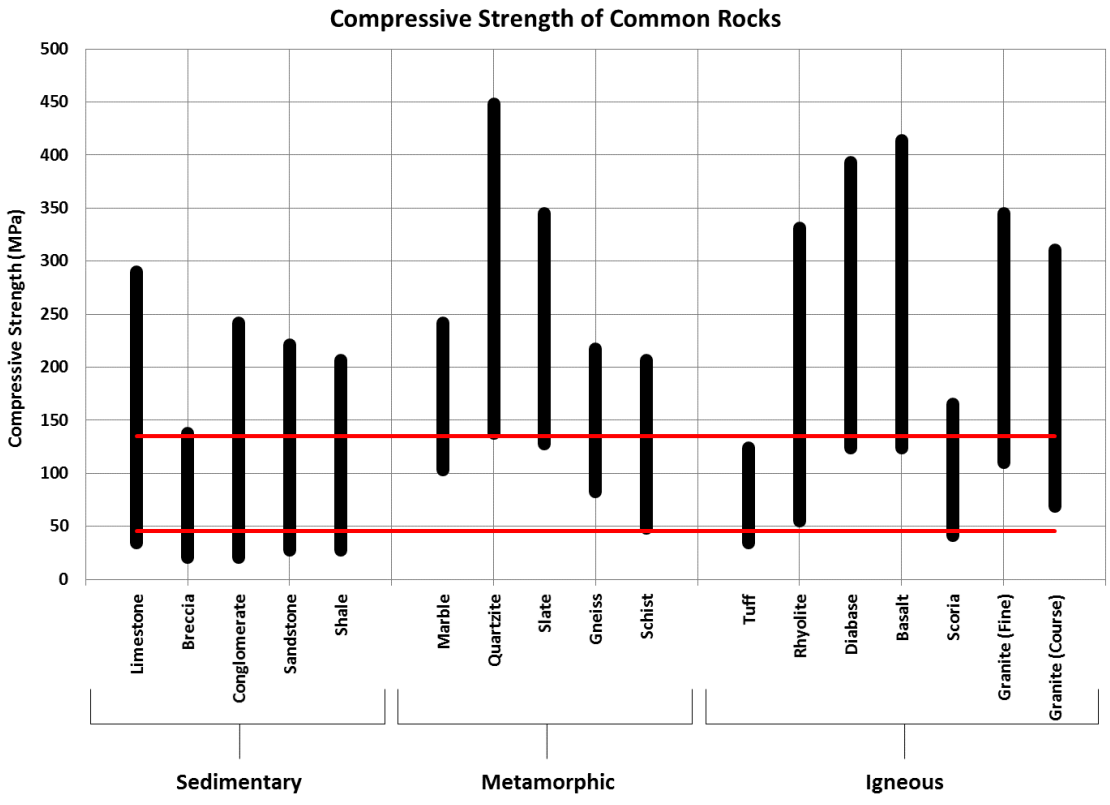

Figure 5.4: Compressive strength of common rocks (adapted from Lowrie, 2002)

The maximum and minimum strengths of the kimberlite were plotted as red lines on Figure 5.4 as a comparison to the compressive strengths of common rock types. As can be seen, the strengths of the kimberlite is similar to scoria and weak granites/rhyolites; it is most applicable to relate the strength of kimberlite to these rocks types as they are also an igneous rock. The complete list of the uniaxial compressive strength test results including the stress-strain graphs for each test can be seen in Appendix C.

5.2.1 Young's Modulus

From the UCS tests both the axial and radial strain was recorded using a data acquisition system. Using the axial strain and stress information, it is possible to determine the Young's modulus of the sample. The Young's modulus is the slope of the axial strain and stress plot at approximately 40% of the UCS or where the curve is most linear. The calculated slope for each sample can be seen in graphical form in Appendix C. The results from the calculations are displayed in Figure 5.5, the results were all fairly similar except MRK and HK, which were much higher than the other rock types.

The second round of testing for MRK indicated a much lower UCS strength and similarly a much lower Young's modulus. As with the lower UCS, the lower Young's modulus is also likely the more accurate value since the samples were larger. The low modulus calculated from the larger MRK core indicate that the rock type is probably less stiff than it was previously thought and in fact is the least rigid of the kimberlites tested. With only a single HK sample for UCS testing, there is little to interpret in the results. However, looking at this single sample, the Young's modulus of HK is quite high compared to the other rock types meaning that HK is a more rigid kimberlite; however, this finding has little strength since it is based on only a single test.

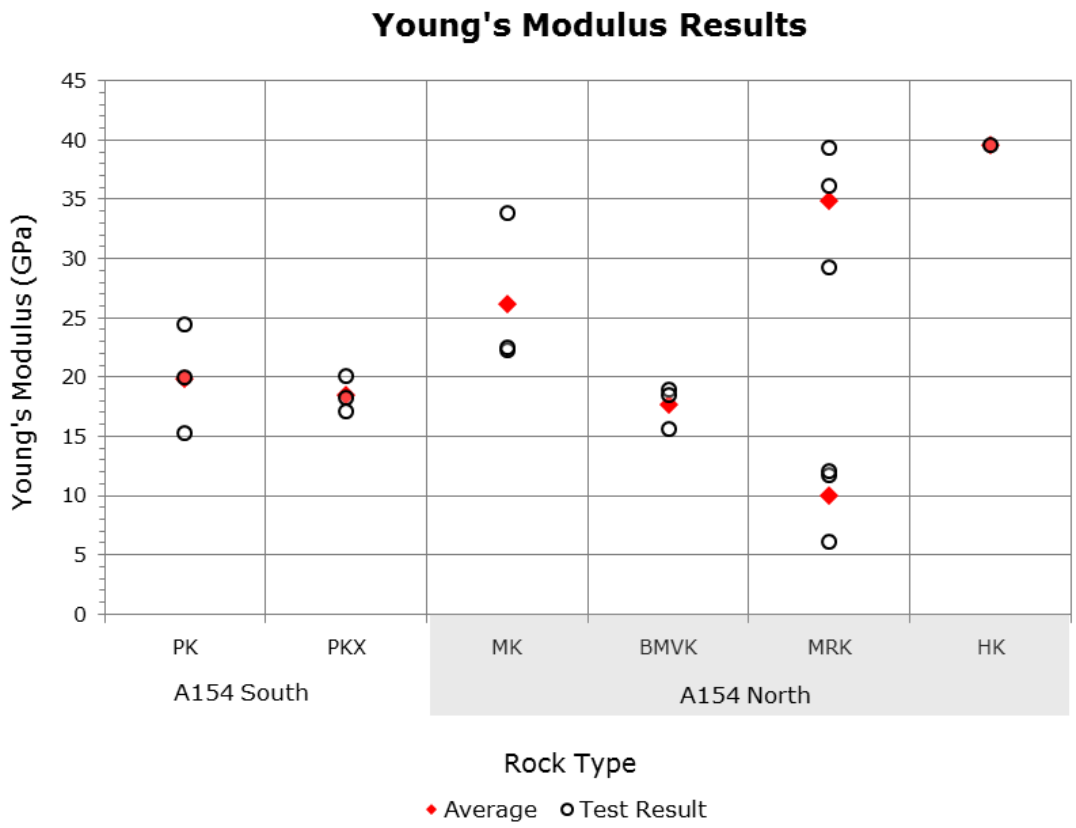

Figure 5.5: Young's modulus results from UCS tests

5.2.2 Poisson's Ratio

The calculation of Poisson's ratio is very similar to Young's modulus. Poisson's ratio is the ratio of the slope of the radial strain curve to the slope of the axial strain curve, or the slope of the radial strain curve to Young's modulus. Poisson's ratio is a measure of the relative expansion and compression in the axial and radial direction of the sample. Most rocks exhibit a Poisson's ratio of approximately 0.24, which can be used as a test of accuracy of the results. The summary of the calculated results are presented in Figure 5.6. The average results were typically close to the 0.24 value; PK and PKX were slightly lower. PK and PKX might be lower than the other rock types because the strain measurements were taken using the compressometer instead of the strain gauges. The large and small MRK cores produced similar average ratios although the deviation of the larger core ratios are considerably greater. The larger deviation could

be attributed to higher sample variability than the smaller cores which would have come from one or two rocks sampled from the same location in the mine. Poisson's ratio is not utilized to determine the rockbursting properties but it is useful to check the performance of the strain measurements and for further research such as numerical modelling of the pipes.

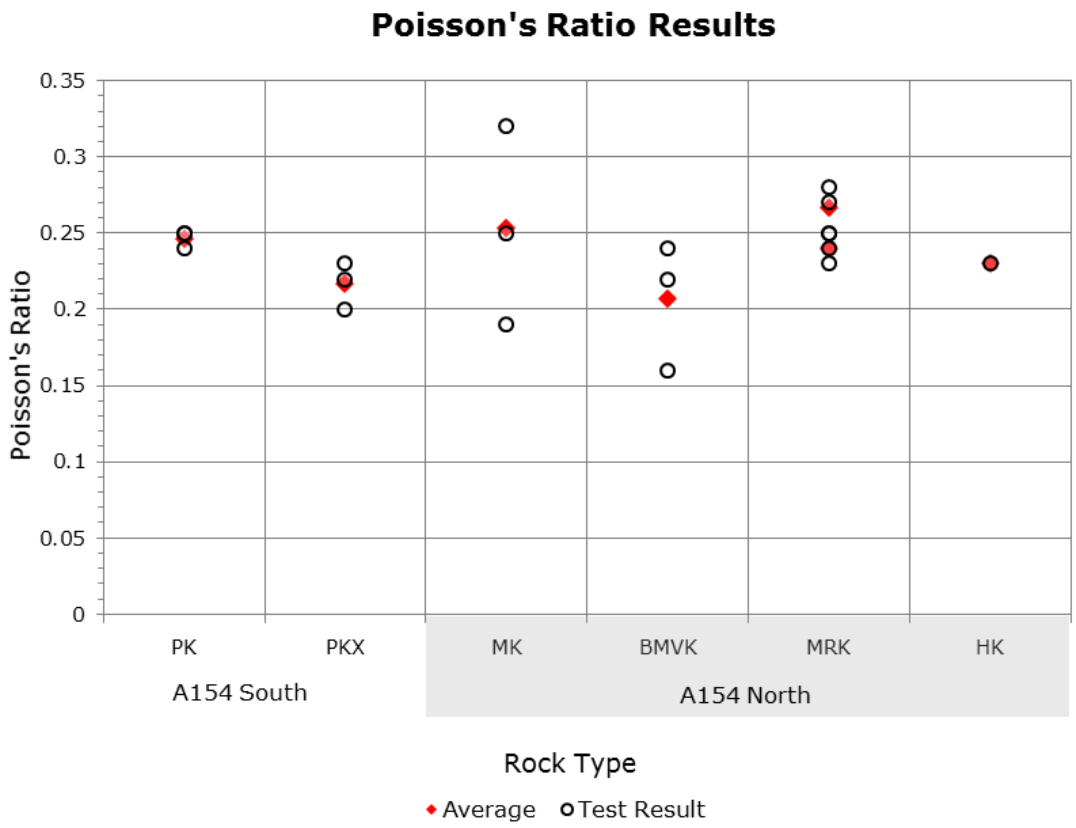

Figure 5.6: Poisson's ratio results from UCS tests

5.3 Hysteresis Loop

The hysteresis loop for each sample was found by performing a cyclic loading test. The samples were loaded and then unloaded in 25 percent increments based on the rock type's UCS until the sample failed. To ensure the sample experienced consistent load cycling, the load was applied and released at the same rate. The information collected from each test looks similar to Figure 5.7; the title MK – UCS4 indicates the rock type and as well as the sample ID, which in this case is UCS4. The figure shows the incremental loading pattern described and the residual strain in the sample when it is unloaded each time. An interesting and an encouraging sign of the measurements quality can be seen when load was reapplied; each time the load was reapplied, the stress-strain curve crossed through the peak of the previous loading cycle indicating that the strain measurement device was still properly attached to the sample.

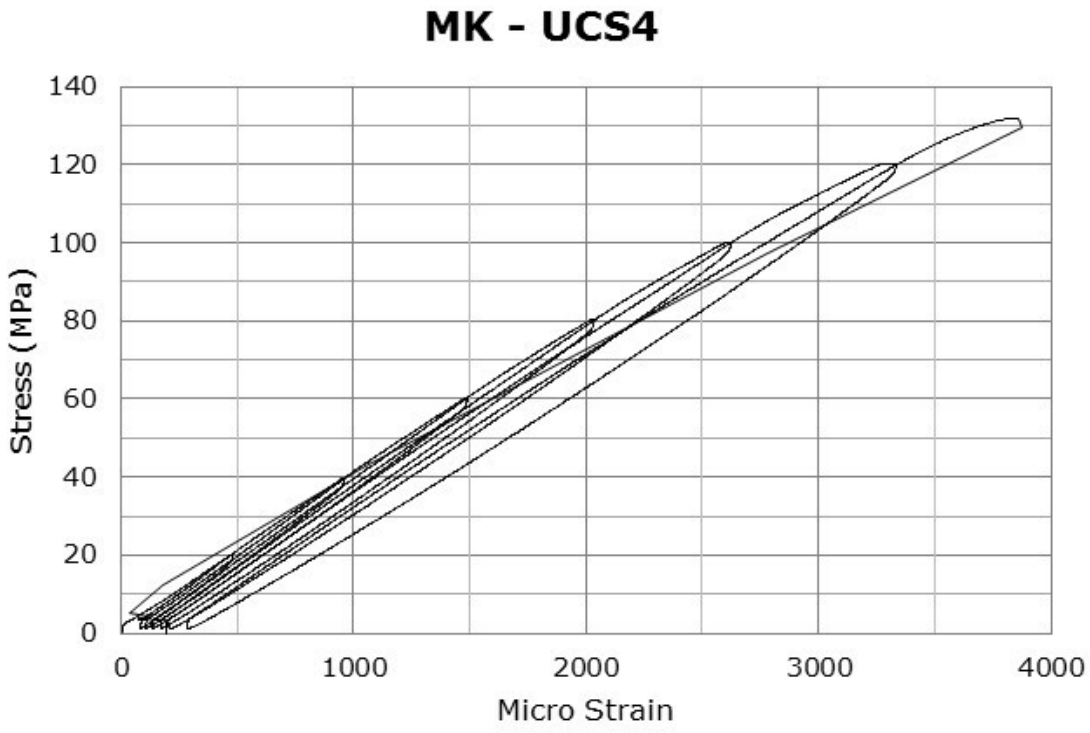

Figure 5.7: Cyclic loading experiment for MK - UCS4

From the information from the graphs similar to Figure 5.7, the data was filtered to the loading cycle which satisfied the 70 to 90% of the ultimate strength of the sample. The data was reduced by removing all the unloading cycles and appending all the loading cycles together to produce the hysteresis loops such as the sample shown in Figure 5.8. All of the filtered hysteresis loops for the samples are in Appendix D. The slope of the unloading curve is also shown on the graph as a red line and represents the unloading modulus, which is used in the determination of the rockbursting properties.

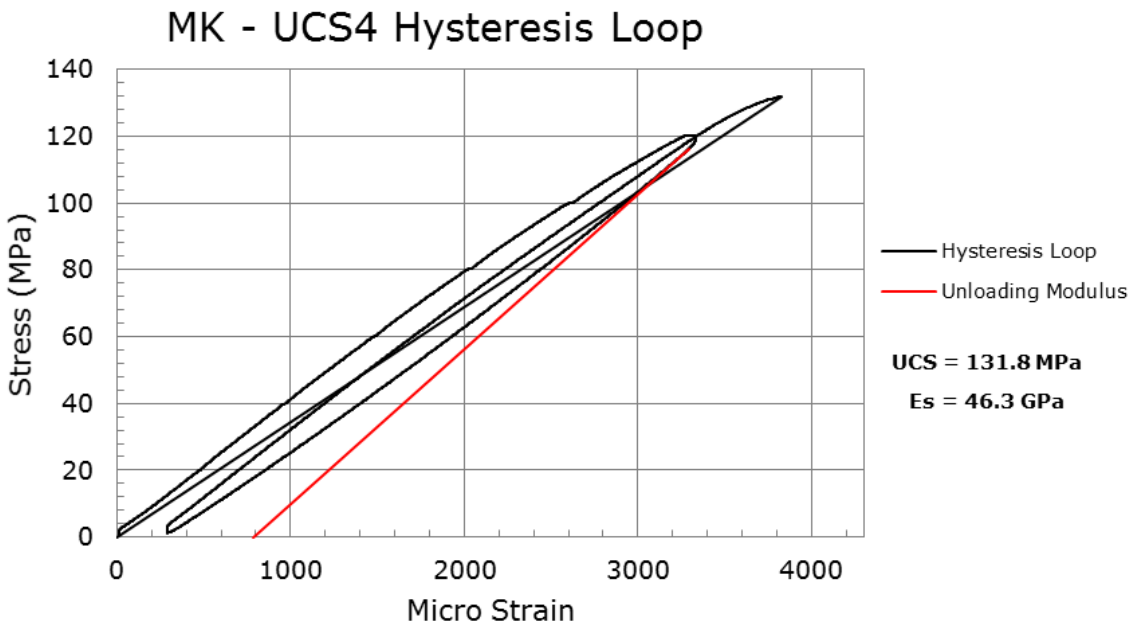

Figure 5.8: Hysteresis loop from cyclic loading test on MK-UCS4

6 Rockburst Analysis

6.1 Strain Energy Index

Utilizing the results from the hysteresis loop tests, the dissipated energy and retained energy areas of the graphs were calculated. The calculated areas are shown in Figure 6.1; the retained energy area is shaded in light grey and the dissipated energy area is shaded in dark grey. Instrument sampling during the experiment occurred at 10 measurement per second, the number of data points being in the thousands simple manual integration through a method of slices was used to determine the area of the shaded regions. The ratio of the retained and dissipated energy areas shown in Figure 6.1 produced a strain energy index value of 5.2. As described in the literature review for the strain energy index method, a result of 5.2 would mean the fragmentation of this rock would be violent and consequently a dangerous rockburst. All of the strain energy index for each sample was determined and the results are shown in Figure 6.2.

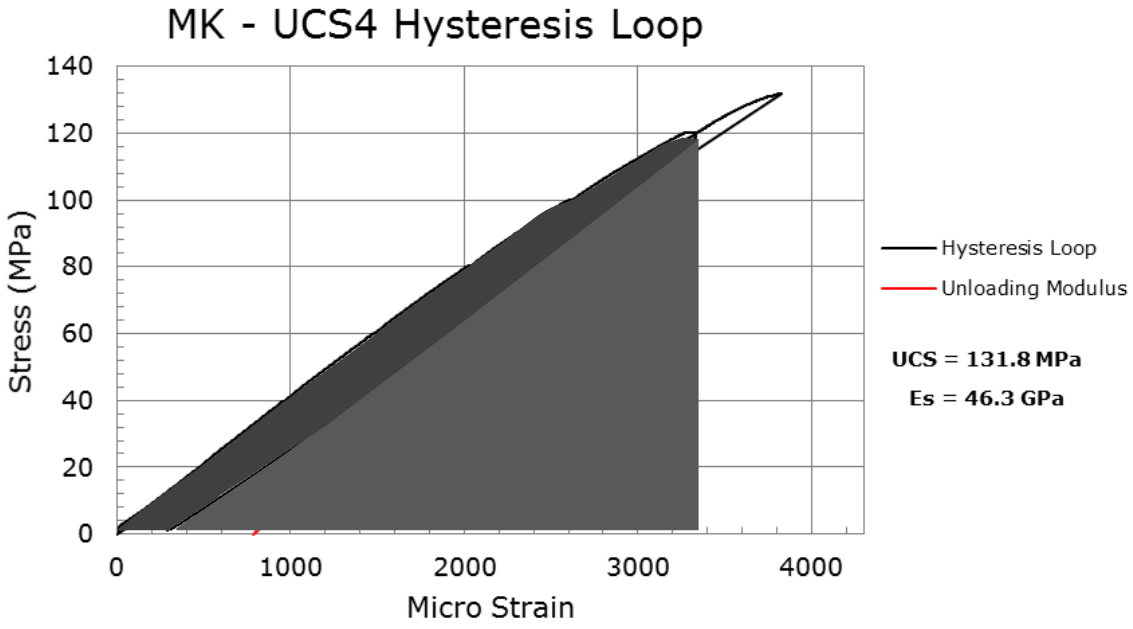

Figure 6.1: Hysteresis loop showing the calculated energy areas

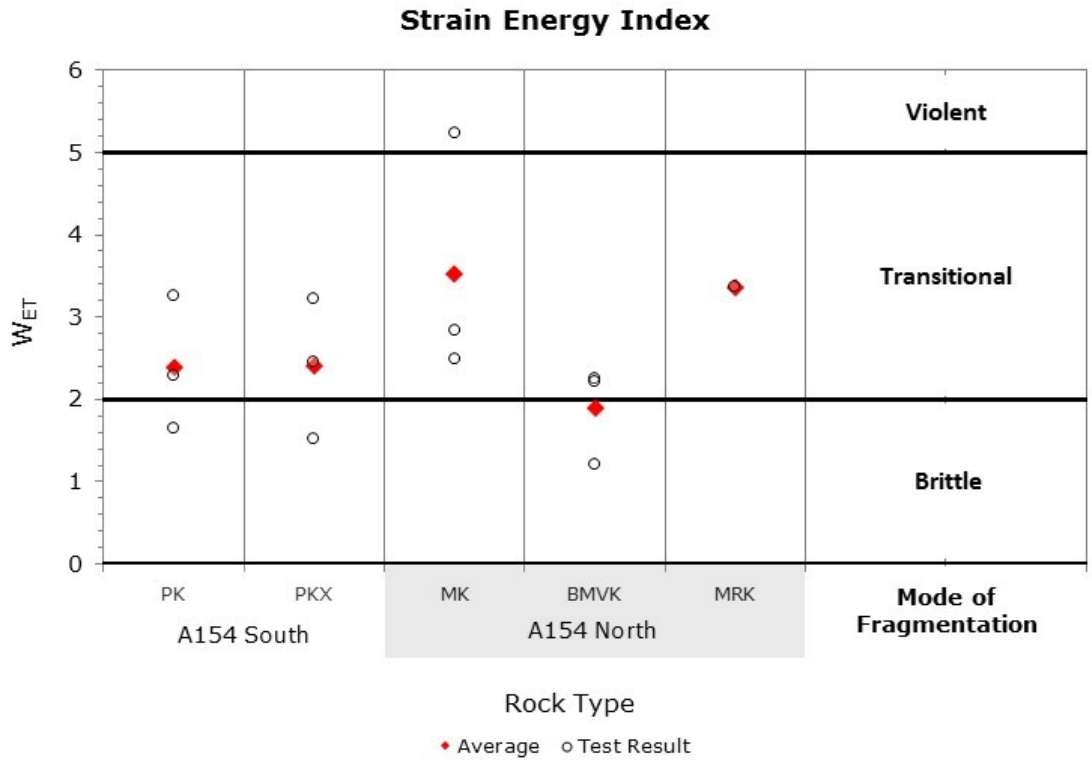

Figure 6.2: Results from strain energy index analysis

The A154 south kimberlite pipe, rock types PK and PKX, produced results that ranged from brittle to transitional fragmentation with the average results falling in the transitional classification. The A154 north pipe showed slightly more variability than the south pipe. The MK rock type displays transitional to violent fragmentation; BMVK exhibited brittle to transitional fragmentation, and MRK only had one successful test that showed transitional fragmentation. The individual results for the strain energy index calculations are listed in Appendix E.

6.2 Strain Energy Density

The results from the hysteresis loops, specifically the unloading modulus, and uniaxial compressive strength tests were used to calculate the strain energy density values for the different rock types. The results from the calculations are shown in Figure 6.3, the rating for the different categories are shown on the right hand side of the graph.

The results show the A154 south pipe had individual results which varied but the results also reveal that the average hazard rating for both rock types were low. A154 north pipe rock types produced a greater variety of ratings. The MK rock type fell between a moderate to high hazard rating; the BMVK was more consistent showing a very low bursting potential, and MRK only produced one complete test with a high hazard rating. A complete list of the unloading modulus, UCS, and the calculated strain energy density value can be found in Appendix E.

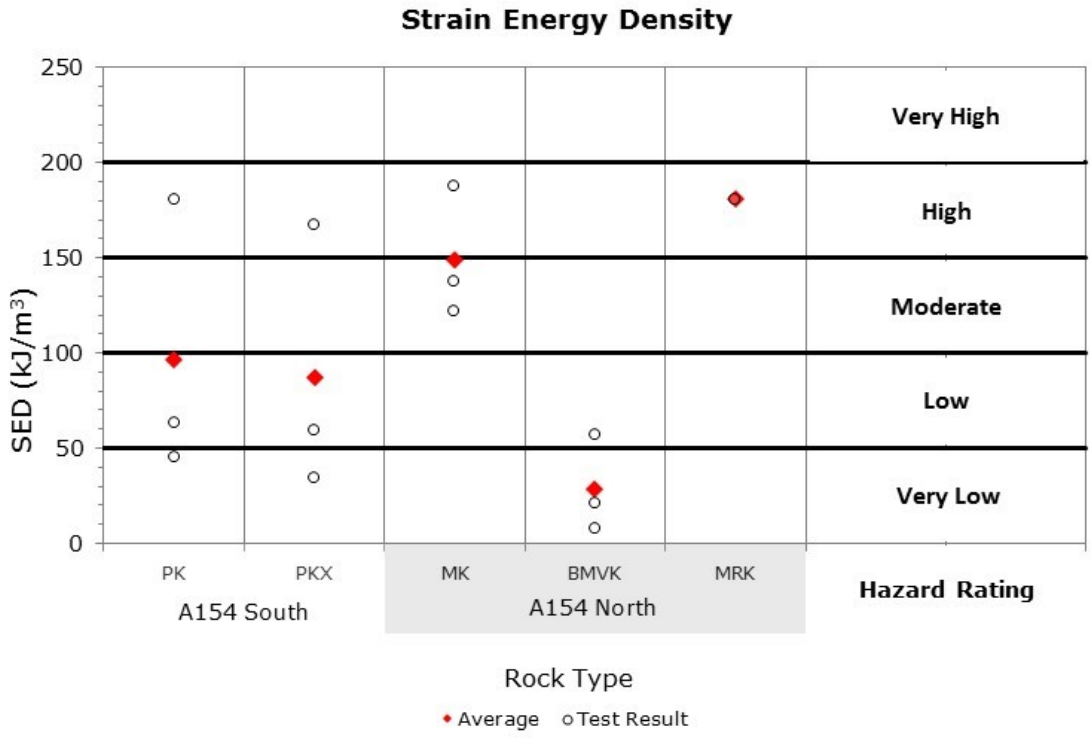

Figure 6.3: Results from strain energy density analysis

6.3 Brittleness Index

The brittleness index estimates the strength of the bursts that a rock will produce. To calculate the brittleness index, the tensile and uniaxial compressive strength values are required. Because there are UCS values from the uniaxial compressive strength tests and the hysteresis loop tests, both were used to calculate the brittleness value. Using both sets of UCS values can help determine if the cyclic loading affected the structure and properties (most importantly strength) of the rock. The results are all shown in Figure 6.4; the averages are shown in red filled and hollow diamonds. The averages from the two UCS data sets are fairly similar for all of the rock types, the biggest range is seen in MK and MRK. The original tests on MRK pointed towards a weak to no burst rating, but the secondary tests on the larger core completely contradicts this finding, indicating that MRK should have a strong to violent strength of burst. All of the brittleness index values are shown in Appendix E.

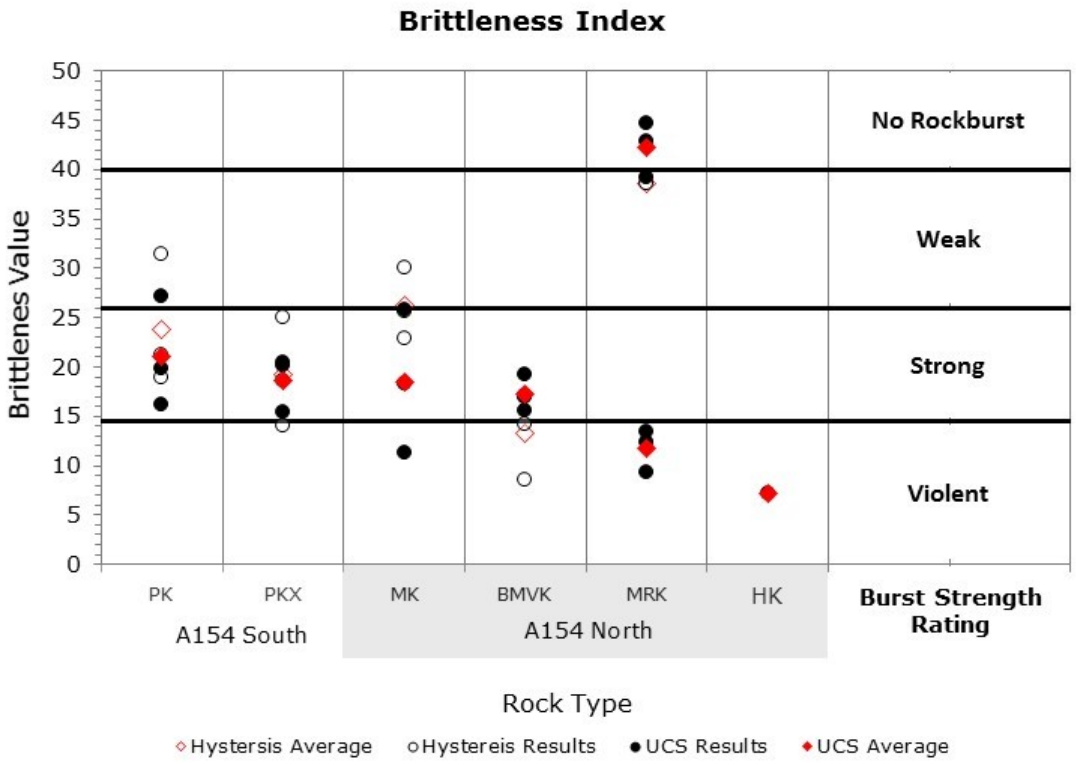

Figure 6.4: Results from brittleness index analysis

6.4 Qualitative Rockburst Properties

The results from the strain energy, strain energy density, and brittleness rockburst analysis methods are summarized in Table 6.1. As can be seen, the A154 south pipe results are the same for both rock types, but the A154 north pipe rock types indicate that the rockbursting properties vary considerably. The variability seen in the north pipe bursting results could be a result of the very different geomechanical properties and geological characteristics. During the mining process the existing stress regimes are altered, and based on the results from the North pipe testing the redistribution of stresses and behaviour of the rock will be considerably different.

Rock Type	W_{ET}	SED	RB
PK	Transitional	Low	Strong
PKX	Transitional	Low	Strong
MK	Transitional	Moderate/High	Strong
BMVK	Brittle	Very Low	Strong
MRK	Transitional	High	Violent
HK	-	-	Violent
VBMK	-	-	-
Average	**Transitional**	**Low/Moderate**	**Strong**

Table 6.1: Summary of rockburst analysis

From the summary of the rockburst analysis a description of the rockbursting properties of each rock type was created, the descriptions can be seen in Table 6.2 Based on the descriptions created from the rockburst analysis it appears that only MK has concerning rockbursting properties. PK, PKX, and BMVK have shown to exhibit low rockbursting danger, and the MRK rock type has almost no concern of rockbursting.

Pipe	Rock Type	Rockburst Properties
A154 South	PK PKX	Low hazard of strong bursts with transitional failure
A154 North	MK	Moderate to high hazard of strong bursts with transitional failure
	BMVK	Very low hazard of strong bursts with brittle failure
	MRK	High hazard of violent bursts with transitional failure
	HK	Unknown hazard and mode of failure, but fails violently

Table 6.2: Description of rockburst properties from the analysis methods

6.5 Combined Rockburst Ratings

The qualitative findings are useful for understanding the nature of the bursting properties of the individual rock types, but comparing the bursting propensity from rock type to rock type is more difficult. To make comparing the rock types more straightforward, the different index methods can be converted into numeric ratings as shown in Table 6.3, giving equal weight to the systems into an average value.

W_{ET}	SED	Brittleness
Brittle = 0	Very Low = 0	No Burst = 0
Transitional = 1	Low = 1	Weak = 1
Violent = 2	Moderate = 2	Strong = 2
	High = 3	Violent = 3
	Very High = 4	

Table 6.3: Rockburst rating conversion system

The calculation of the combined rockburst rating is done by dividing the three individual rating systems by the maximum respective index value, taking an equal weighted average of the results and then finally multiplying 100 to create a rating out of 100. The closer the combined rating is to 100, the greater the rockburst concern. An example of the calculation can be seen below for rock type PK and the summary of the calculations for all the rock types in Table 6.4.

$$Combined\ Rating = \ Average\left[\left(\frac{1}{2}\right), \left(\frac{1}{4}\right), \left(\frac{2}{3}\right)\right] * 100$$

$$Combined\ Rating = Average[0.5, 0.25, 0.667] * 100$$

$$Combined\ Rating = 0.47 * 100$$

$$Combined\ Rating = \mathbf{47}$$

Pipe	Rock Type	W_{ET}	SED	Brittleness	Combined Rating (out of 100)
A154 South	PK	1	1	2	47
	PKX	1	1	2	47
A154 North	MK	1	2.5	2	60
	BMVK	0	0	2	28
	MRK	1	3	3	75
	HK	-	-	3	100*
Average		1	1.5	2	68

*Based on only brittleness index

Table 6.4: Combined ratings for all rock types

Looking at the results of the combined ratings in Table 6.4, it is much easier to compare the rockbursting propensity of the different rock types. The results from HK indicate that it is highly burst prone, although this is based on very little data and therefore, not very reliable. Analyzing the other rock types, the order of burst propensity from high to low are as follows: MRK, MK, PK, PKX, and BMVK; with PK and PKX having the same combined rating. The MRK rock type has the highest rockburst rating and therefore will be the most likely to exhibit rockbursting behaviour. MK also has a very high combined rating, but the other rock types (PK, PKX, and BMVK) all have ratings less than 50, meaning that they are much less likely to produce bursts.

6.6 Rockburst Mapping

Rockburst maps can be created to highlight the different ratings of the different rock types and spatial relations. Two cross-section examples of such maps can be seen in Figure 6.5. The maps show the greater variety in the rockburst rating found in the North pipe compared to the South pipe. The areas of the pipe that are not filled in represent areas with unknown rockburst properties. These maps provide a valuable tool to mitigate rockbursts from occurring during the planning process. While planning, a planner can determine an optimal approach and sequencing for the level based on the rockburst ratings.

Analyzing the North pipe map, based on the changing rockburst rating, development and mining of this level would be more difficult. As mining proceeds, the changing rock types will react differently to the changing stress regime. For instance, as the HK portion of this level is mined, there would be a much higher probability of encountering a rockburst than in the MK areas.

The sample rockburst map of the South pipe would be less critical to the mine design for the level since the rockburst rating is the same for the known rock types. The map is still useful as it provides information on the combined rating, which could be very important depending on the rating.

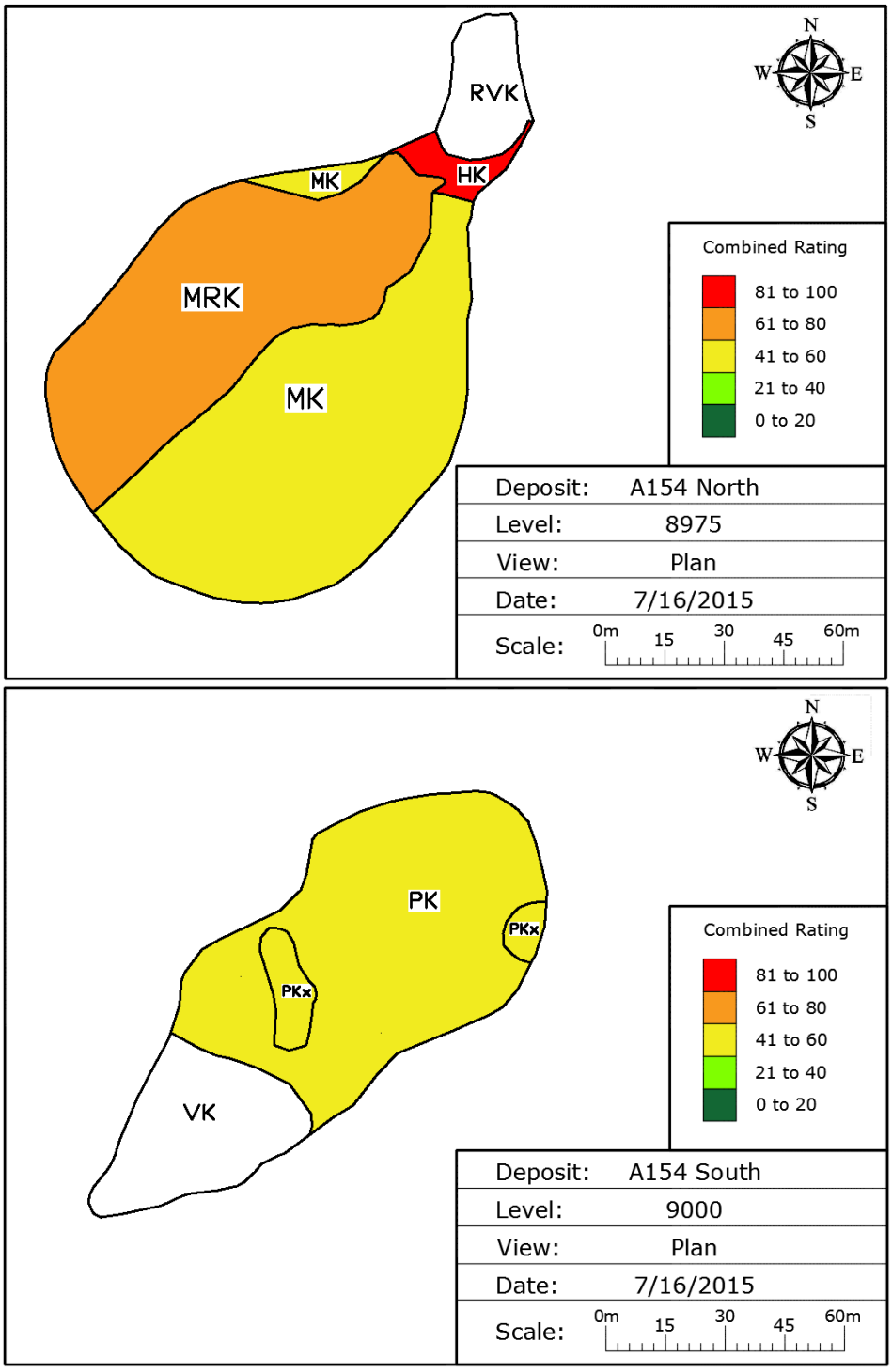

Figure 6.5: Combined ratings cross-sections for north and south pipe rock types

6.7 Pipe Volumes & Rockburst Rating

The combined rockburst ratings determined can also be combined with the rock type percentages detailed in section 3.1.3 Rock Types at Diavik to better understand the amount of each pipe that will cause difficulties. Figure 6.6 and Figure 6.7 show the relative volume percentage of each of the rock types in the South and North pipes respectively with each rock type coloured based on their appropriate combined rockburst rating.

The South pipe's rock type volumes and the combined rockburst rating is shown in Figure 6.6. As it has been noted before, both the rock types tested from the South pipe produced very similar rockbursting properties and consequently identical combined rockburst rating. Another interesting finding from the graph is the volume of the South pipe with unknown rockburst properties. Testing on the PK and PKX provided rockbursting information on 63% of the pipe, but still 37% of the pipe's properties remain unknown.

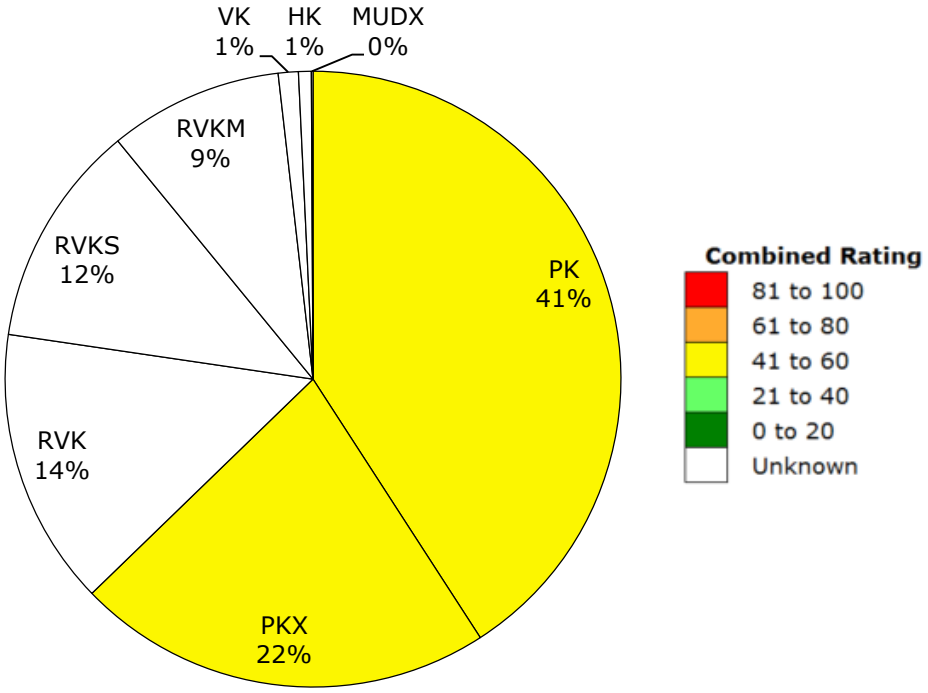

Figure 6.6: A154 South rock type breakdown indicating combined rockburst rating

Figure 6.7 shows the rock type volumes for the North pipe with the combined rockburst ratings indicated. The rockburst ratings are notably more varied in the North pipe. A majority of the pipe have a combined rockburst rating of 60 indicated by the yellow shading. MRK comprises 22% of the pipe and has a rating of 75, BMVK 5% with a rating of 28, and finally the 2% HK rated at 100; although the HK rating was based only on the brittleness index. Because more rock types were tested, a considerable greater amount of the North pipe is known compared to the South pipe. In total 83% of the North pipe's bursting properties are known, with only 17% of the pipe unknown.

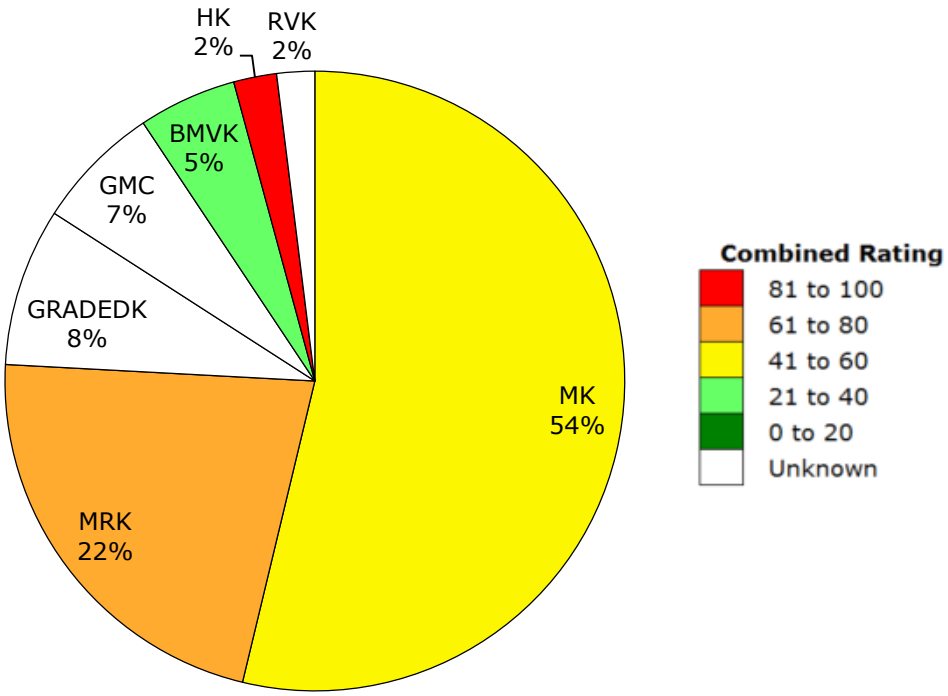

Figure 6.7: A154 North rock type breakdown indicating combined rockburst rating

7 Conclusion

Rockbursts are a natural phenomenon that can be exacerbated by the activities of mineral extraction. When a rockburst occurs, large quantities of stored energy is released from the rock causing it to be expelled from the face of an underground opening. There has been great research done in terms of identifying rockburst prone materials through the properties of the rocks, but there are still many rock types whose potential for bursting is unknown. The diamond bearing rock, kimberlite, is one rock that has little known of its rockbursting properties. The strain energy index, strain energy density, and rock brittleness methods are the three methods that were employed to deduce the bursting potential of kimberlite.

Tests were conducted on six different types of kimberlite collected from a Canadian diamond mine including: uniaxial compression tests, Brazilian tests, and cyclic loading tests. The samples tested were from two different pipes identified by A154 North and A154 South. Merging the results from the three rockburst prediction methods, it was found that the bursting potential varied for each type of kimberlite. Overall the A154 South pipe had a lower rockburst potential on the combined rating system and is not likely to have problem with rockbursts. The North pipe showed that it had a much higher probability of bursts occurring, predominantly in the MRK, MK, and HK rock types. Therefore, the findings indicate that not all kimberlite is prone to bursting, but rather certain kinds of kimberlite, as its composition and characteristics are relatively diverse.

The findings from the research are very useful but there are also some limitations that are equally important. The rockburst prediction methods that were used were developed based on studies of coal and granite rocks. The properties of kimberlite generally falls between coal and granite, but this does not mean that the results will be accurate. Furthermore, the prediction methods employed in this study do not take into account the depth of the deposit and current stress regimes. Another limitation of the research is the number of samples that were tested and the variety of deposits upon which the findings are founded. The sampling method also potentially creates a bias in the results. Typically for this kind of study the best possible samples are collected and in this case the same rock types would have been collected from the

same part of the mine. Therefore, the findings might be strongly spatially correlated to the specific regions of the pipes from which the samples were taken.

8 Future Research

Although this study provided new insight into the rockbursting properties of kimberlite, there are still many areas for future research on the topic. Firstly, if possible a greater number of samples from different levels of mine can be tested to ensure the repeatability of the findings and a greater grasp of the spatial correlation of the data. Testing samples from other kimberlite deposits would also help to create a better understanding of the bursting properties of kimberlite in general. Secondly, using other burst prediction methods, such as the tangential stress method, that take would into consideration the stresses of the different rock types to better isolate the locations that will create rockbursts. To utilize the tangential stress method, it would require knowledge of the horizontal to vertical stress ratio of the rock mass. This additional information was not available during this study, but would help in understanding the rockburst properties. Another method that could be used on a broader scale is including the RQD method. The RQD method takes into consideration the overall rockmass quality; this would help to alleviate some of the bias that is inherent in making macro scale assumptions of an orebody based solely on core testing. Lastly, an excellent area of future research would be in the creation of a bursting index system based on kimberlite instead of granite or coal. Creating a kimberlite bursting index could be accomplished by combining qualitative data from mines describing rockbursts in a rock type and the laboratory measurements of the rock type properties from tests such as those conducted in this study.

References

Bennett, T. J., & Marshall, M. E. (2001). *Identification of rockbursts and other mining events using regional signals at international monitoring system stations.* Science Applications International Corporation.

Blake, W., & Hedley, D. G. (2003). *Rockbursts: Case Studies from North American Hard-Rock Mines.* USA: Society for Mining, Metallurgy, and Exploration.

Cook, N. G. (1983). Origin of rockbursts. In T. I. Metallurgy, *Rockbursts: prediction and control* (pp. 1-2). London: Barnes Design and Print Group.

Diavik Diamond Mine. (2012). *2012 Sustainable Development Report.* Retrieved from http://www.diavik.ca/documents/2012_Sustainable_Development_Report.pdf

Fomradas, G. (2015, 07 18). Rock type percentage breakdown of Diavik diamond pipes. (P. Leveille, Interviewer)

Ge, M. (2005). Efficient mine microseismic monitoring. *International Journal of Coal Geology*, 44-56.

Hedley, D. G. (1992). *Rockburst Handbook for Ontario Hardrock Mines.* Ottawa: Canada Communication Group.

Kidybinski, A. (1981). Bursting Liability Indices of Coal. *International Journal of Rock Mechanics, Mineral Sciences & Geomechanics*, 295-304.

Lowrie, R. L. (2002). *SME Mining Reference Handbook.* US: Society for Mining, Metalurgy, and Exploration.

Magill, F. N. (1990). *Magill's Survey of Science - Earth Science Series.* Pasadena: Salem Press.

Perras, M. A., & Diederichs, M. S. (2014). A Review of the Tensile Strength of Rock: Concepts and Testing. *Geotechnical and Geological Engineering*, 525-546.

Rio Tinto. (2015). *Photo Library - Rio Tinto*. Retrieved from http://www.riotinto.com/media/photo-library-263.aspx?y=1492

Rowmanowski, J. (2014). Diavik Diamond Mine Underground. (P. Leveille, Interviewer)

Salamon, M. (1984). Energy considerations in rock mechanics: fundamental results. *Journal of the South African Institute of Mining and Metallurgy*, 233-246.

Wang, J.-A., & Park, H. (2001). *Comprehensive prediction of rockburst based on analysis of strain energy in rocks.* Seoul: Elsevier Science Ltd.

Wattimena, R. K., Sirait, B., Widodo, N. P., & Matsui, K. (2012). Evaluation of rockburst potential in a cut-and-fill mine using energy balance. *International Journal of the Japanese Committee for Rock Mechanics*, 19-23.

Appendix A Sample Measurements

Pipe	Rock Type	Sample ID	Diameter (mm)	Thickness (mm)	Thickness to Diameter
A514 North	HK	T1	63.30	26.63	0.42
		T2	63.50	26.64	0.42
		T3	63.54	24.94	0.39
		T4	63.38	26.65	0.42
		T5	63.54	26.58	0.42
	MRK	T1	37.51	18.64	0.5
		T2	37.51	18.24	0.49
		T3	37.56	19.79	0.53
		T4	62.85	26.31	0.42
		T5	62.87	26.22	0.42
		T6	62.87	26.72	0.43
	MK	T1	38.07	20.65	0.54
		T2	37.83	20.47	0.54
		T3	37.79	20.41	0.54
		T4	37.89	20.79	0.55
		T5	37.98	20.42	0.54
		T6	37.96	20.59	0.54
	BMVK	T1	38.11	22.57	0.59
		T2	38.11	23.24	0.61
		T3	38.13	23.65	0.62
		T4	38.11	22.71	0.6
		T5	38.07	22.74	0.6
		T6	38.09	23.53	0.62
		T7	38.15	21.26	0.56
A154 South	PK	T1	63.28	38.05	0.6
		T2	63.30	38.07	0.6
		T3	63.32	37.92	0.6
	PKX	T1	63.32	38.54	0.61
		T2	63.27	38.44	0.61
		T3	63.34	38.77	0.61
		T4	37.99	21.73	0.57
		T5	38.01	22.16	0.58
		T6	38.01	22.50	0.59
		T7	37.90	22.26	0.59
A418	VBMK	T1	37.91	22.91	0.6
		T2	38.06	22.28	0.59
		T3	38.07	23.27	0.61
		T4	38.11	24.03	0.63
		T5	38.02	23.00	0.61
		T6	38.12	22.18	0.58
		T7	37.97	23.28	0.61
		T8	38.08	22.66	0.6

*Grey shading indicates second set of testing

Table A.1: Brazilian sample measurements

Pipe	Rock Type	Sample ID	Length (mm)	Diameter (mm)	Length to Diameter	Area (mm^2)
A154 South	PK	UCS1	129.06	63.30	2.0	3147
		UCS2	128.59	63.38	2.0	3155
		UCS3	117.69	63.36	1.9	3153
	PKX	UCS1	132.52	63.37	2.1	3154
		UCS2	131.01	63.29	2.1	3146
		UCS3	127.71	63.42	2.0	3159
A154 North	MK	UCS1	88.12	37.78	2.3	1121
		UCS2	88.18	37.85	2.3	1125
		UCS3	88.98	37.94	2.3	1130
	HK	UCS1	128.49	63.41	2.0	3158
	BMVK	UCS1	88.02	38.07	2.3	1138
		UCS2	87.77	38.02	2.3	1136
		UCS3	87.74	38.00	2.3	1134
	MRK	UCS1	83.78	38.02	2.2	1135
		UCS2	72.99	37.95	1.9	1131
		UCS3	84.90	38.08	2.2	1139
		UCS4	131.27	62.87	2.1	3105
		UCS5	139.55	62.98	2.2	3115
		UCS6	133.75	61.11	2.2	2933

*Grey shading indicates second set of testing

Table A.2: Uniaxial compressive strength sample measurements

Pipe	Rock Type	Sample ID	Length (mm)	Diameter (mm)	Length to Diameter	Area (mm^2)
A154 South	PK	UCS4	132.75	63.36	2.1	3153
		UCS5	73.52	37.66	2.0	1131
		UCS6	73.03	37.77	1.9	1120
	PKX	UCS4	128.38	63.29	2.0	3146
		UCS5	81.76	37.95	2.2	1131
		UCS6	87.28	37.95	2.3	1131
A154 North	MK	UCS4	87.38	37.96	2.3	1132
		UCS5	88.78	37.83	2.3	1124
		UCS6	88.52	38.06	2.3	1138
	BMVK	UCS4	87.88	38.11	2.3	1141
		UCS5	87.20	38.06	2.3	1138
		UCS6	88.02	38.11	2.3	1141
	MRK	UCS4	77.77	37.99	2.0	1134
		UCS5	77.01	37.91	2.0	1129
		UCS6	80.43	37.29	2.2	1092

Table A.3: Hysteresis loop sample measurements

Appendix B Brazilian Tensile Strength Test

Pipe	Rock Type	Sample ID	Max Load (KN)	σ_T (MPa)
A514North	HK	T1	29.4	11.1
		T2	20.2	7.6
		T3	14.4	5.8
		T4	42.7	16.1
		T5	21.6	8.2
	MRK	T1	4.3	3.9
		T2	3.2	3.0
		T3	3.1	2.7
		T4	6.3	2.4
		T5	12.9	5.0
		T6	11.4	4.3
	MK	T1	5.7	4.7
		T2	6.8	5.6
		T3	4.8	4.0
		T4	2.5	2.0
		T5	6.7	5.5
		T6	5.5	4.5
	BMVK	T1	7.4	5.5
		T2	5.1	3.7
		T3	4.9	3.5
		T4	3.4	2.5
		T5	4.3	3.1
		T6	1.1	0.8
		T7	2.6	2.0
A154 South	PK	T1	10.0	2.6
		T2	10.7	2.8
		T3	13.6	3.6
	PKX	T1	15.3	4.0
		T2	12.5	3.3
		T3	13.7	3.5
		T4	3.1	2.4
		T5	5.4	4.0
		T6	5.0	3.7
		T7	6.8	5.2
A418	VBMK	T1	1.2	0.9
		T2	7.7	5.8
		T3	2.0	1.4
		T4	8.7	6.0
		T5	10.7	7.8
		T6	2.6	2.0
		T7	2.1	1.5
		T8	3.2	2.4

*Grey shading indicates second set of testing

Table B.1: Brazilian tensile strength test results

Appendix C Uniaxial Compressive Strength Test

Pipe	Rock Type	Sample ID	UCS (MPa)	E (GPa)	Poisson's Ratio
A154 South	PK	UCS1	49.1	15.3	0.25
		UCS2	60.0	20.0	0.25
		UCS3	82.2	24.4	0.24
	PKX	UCS1	74.8	20.1	0.22
		UCS2	76.0	18.3	0.20
		UCS3	57.3	17.1	0.23
A154 North	MK	UCS1	112.6	33.8	0.25
		UCS2	79.9	22.3	0.19
		UCS3	49.5	22.5	0.32
	HK	UCS1	70.4	39.6	0.23
	BMVK	UCS1	65.1	19.0	0.22
		UCS2	52.8	18.5	0.24
		UCS3	57.1	15.6	0.16
	MRK	UCS1	142.5	39.4	0.23
		UCS2	124.9	29.3	0.24
		UCS3	136.6	36.1	0.25
		UCS4	52.5	11.7	0.28
		UCS5	48.0	12.1	0.27
		UCS6	36.4	6.1	0.25

*Grey shading indicates second set of testing

Table C.1: Uniaxial compressive strength test results

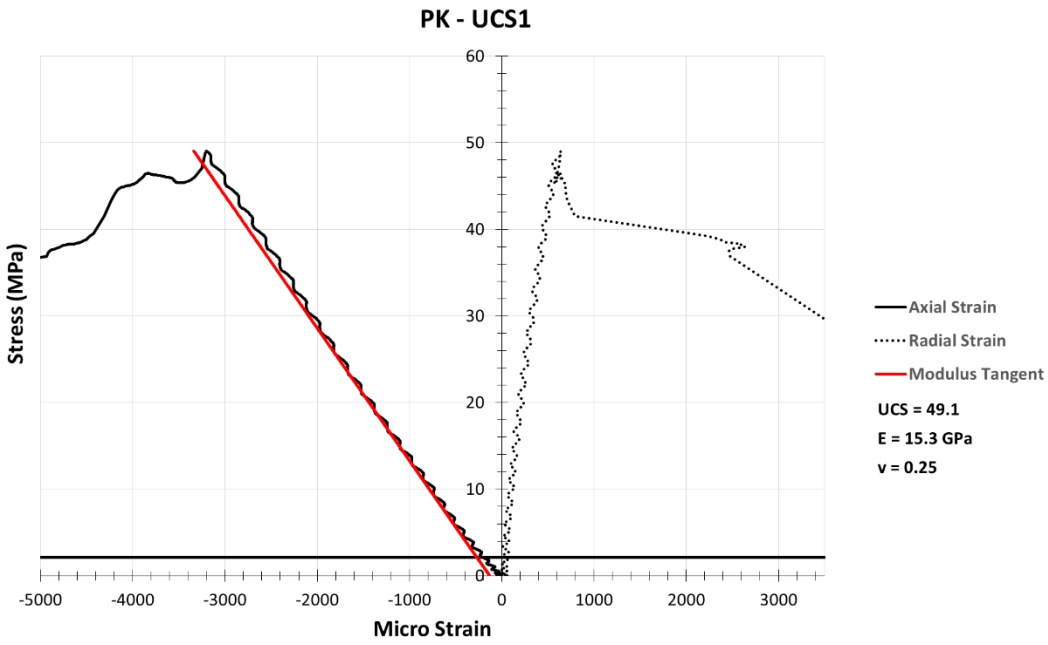

Figure C.1: PK – UCS1 stress vs strain plot

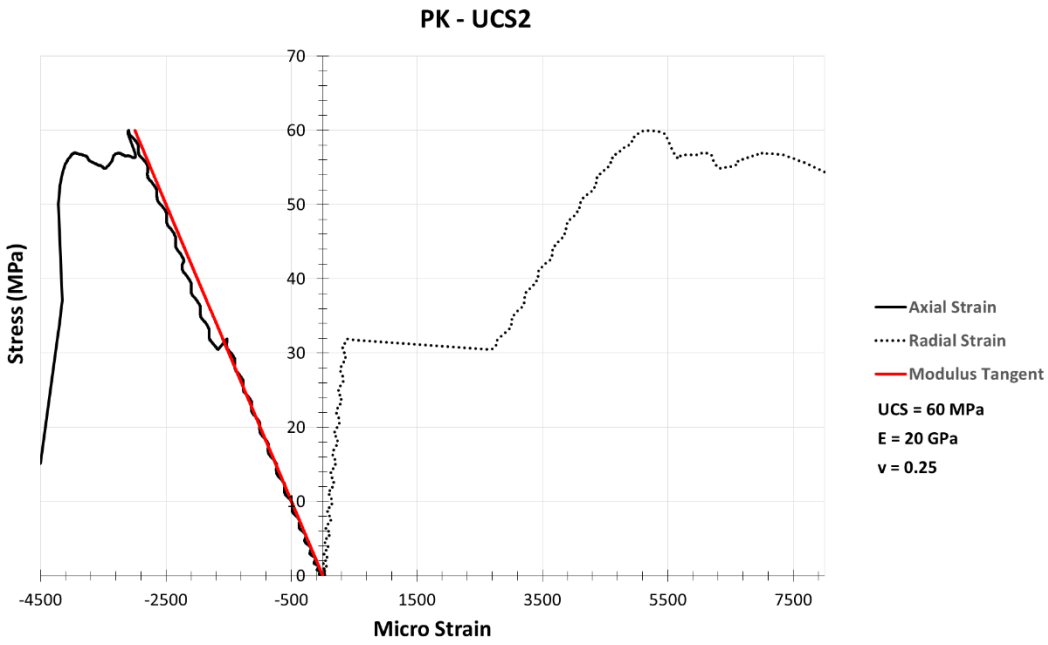

Figure C.2: PK – UCS2 stress vs strain plot

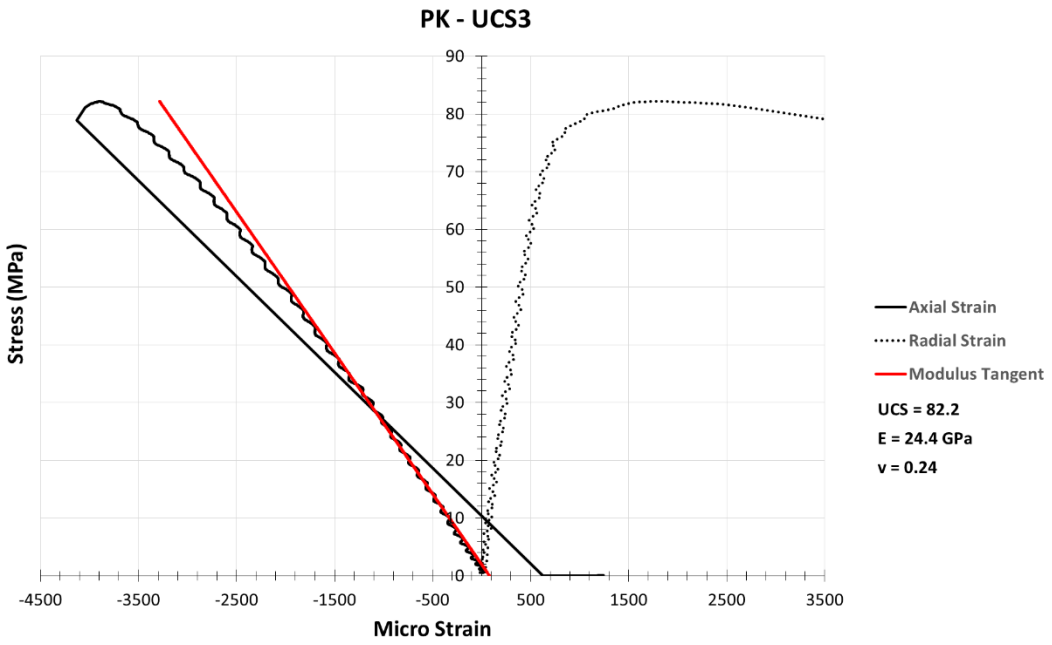

Figure C.3: PK – UCS3 stress vs strain plot

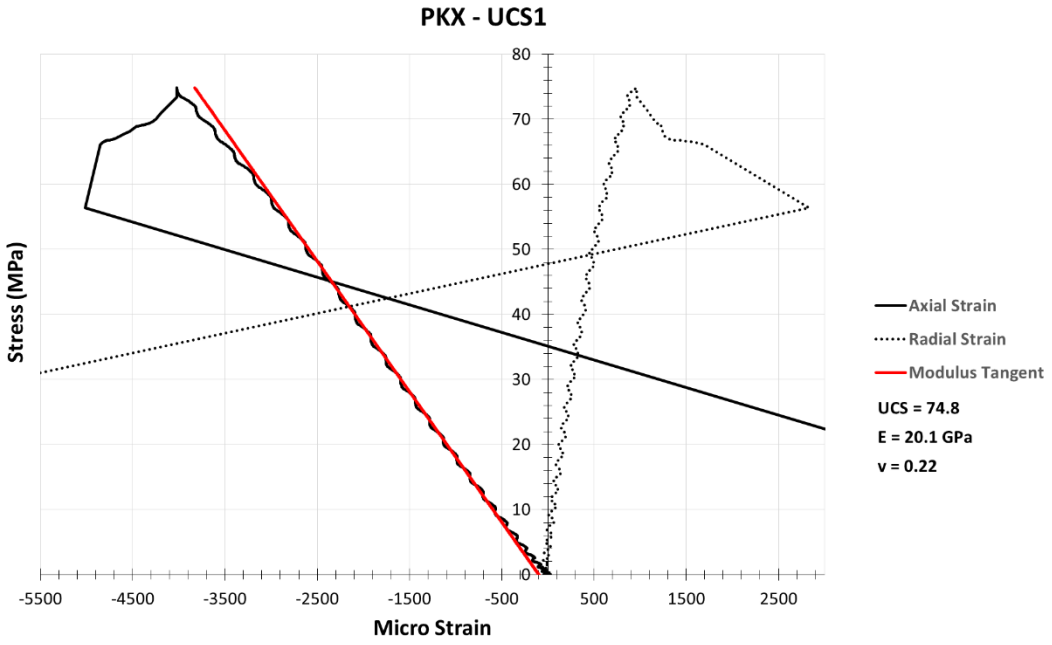

Figure C.4: PKX – UCS1 stress vs. strain plot

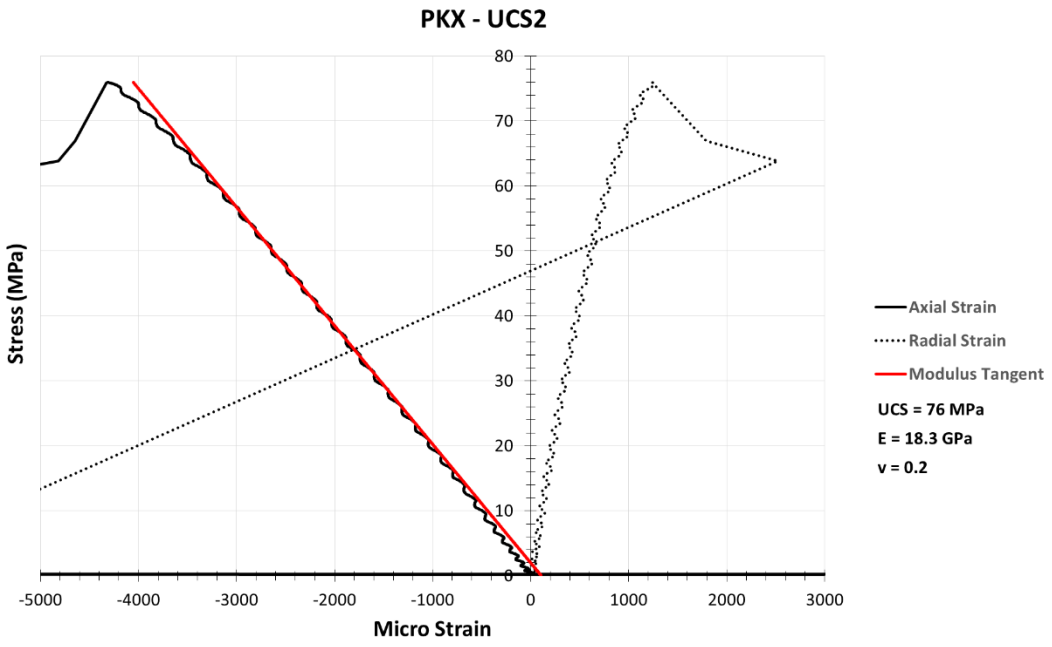

Figure C.5: PKX – UCS2 stress vs. strain plot

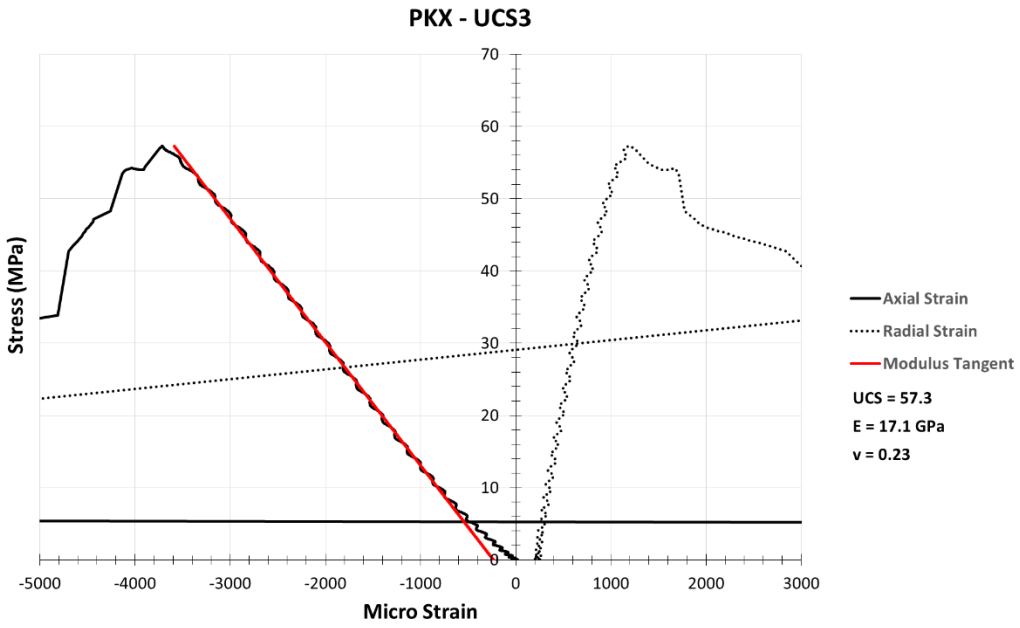

Figure C.6: PKX – UCS3 stress vs. strain plot

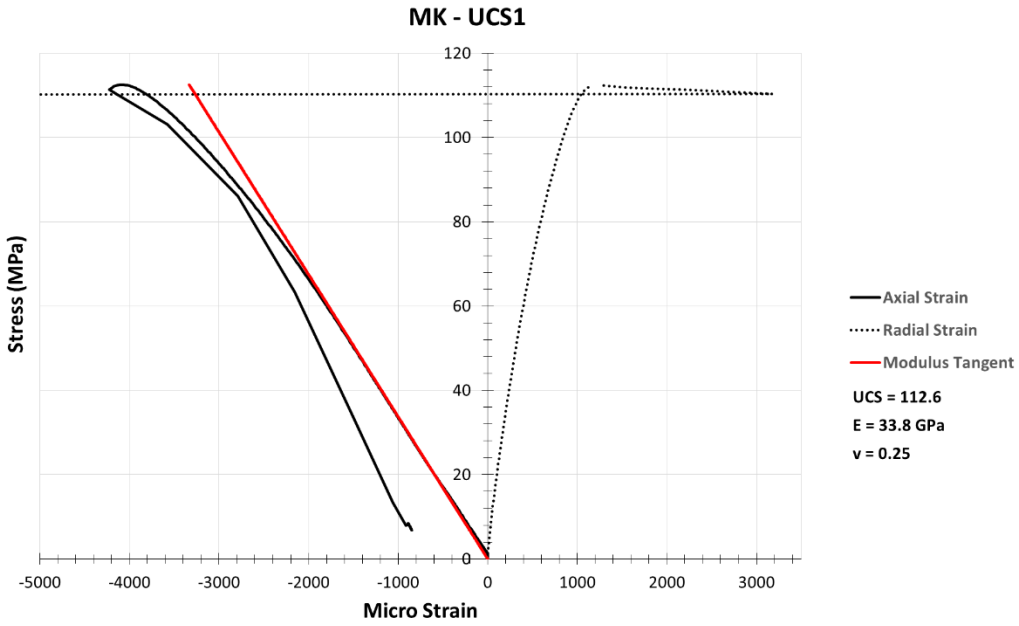

Figure C.7: MK – UCS1 stress vs. strain plot

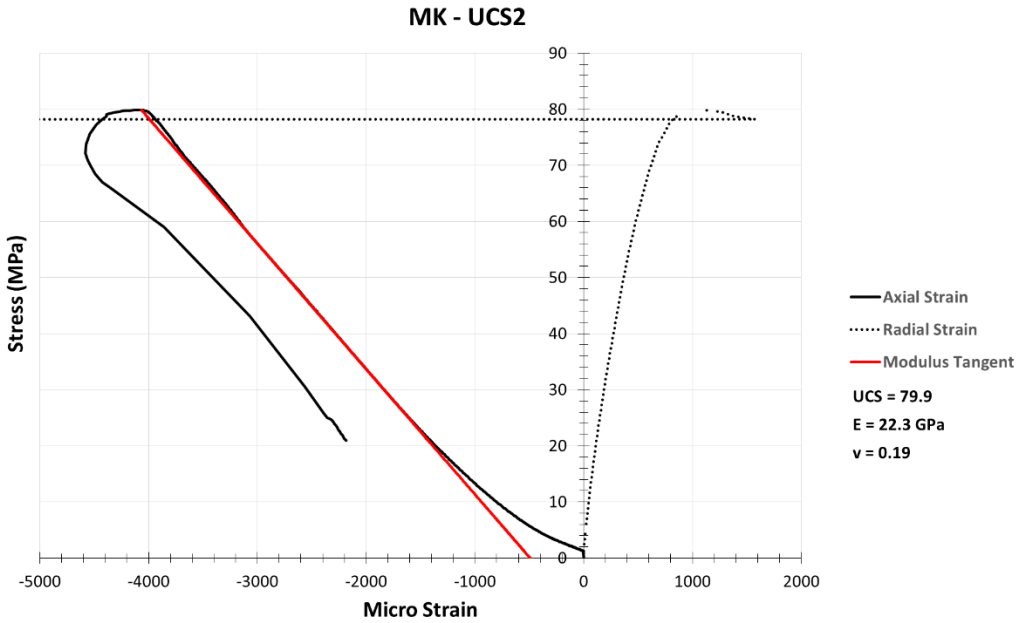

Figure C.8: MK – UCS2 stress vs. strain plot

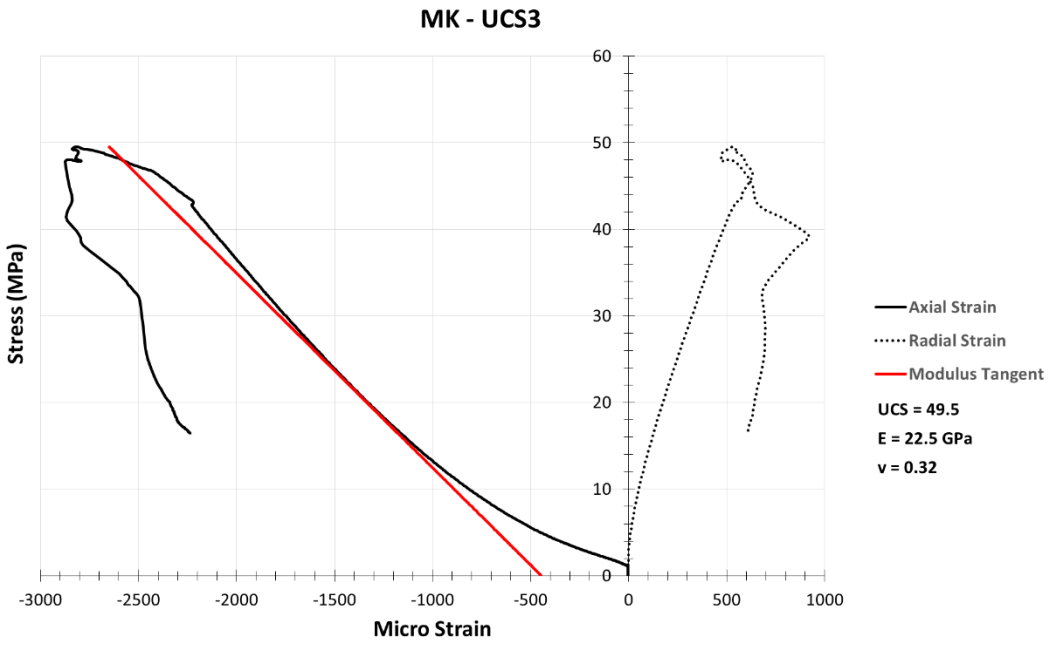

Figure C.9: MK – UCS3 stress vs. strain plot

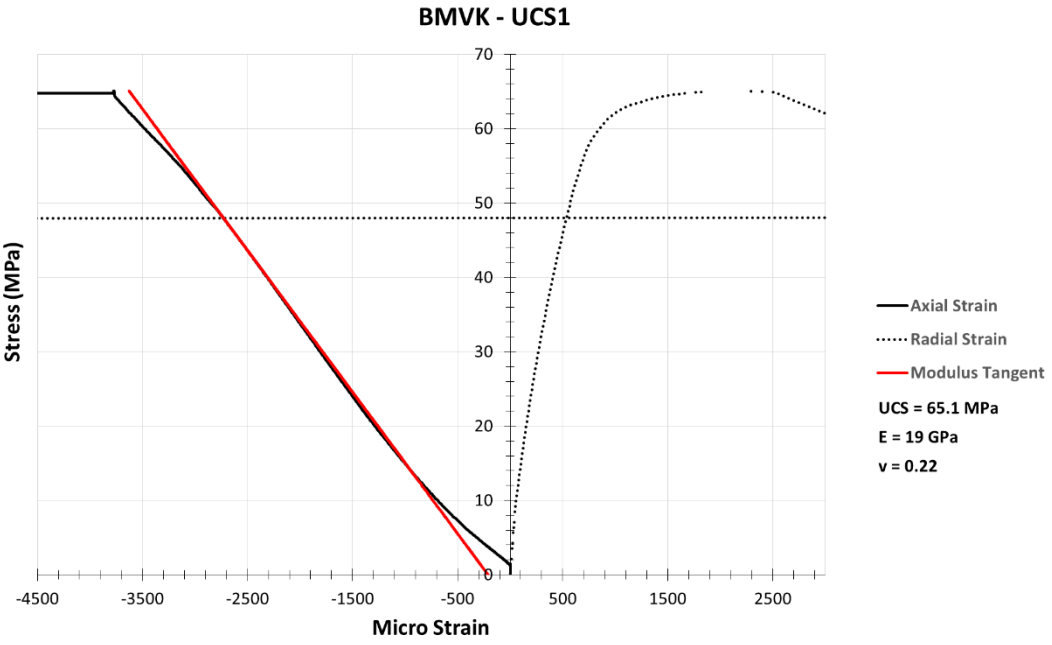

Figure C.10: BMVK – UCS1 stress vs. strain plot

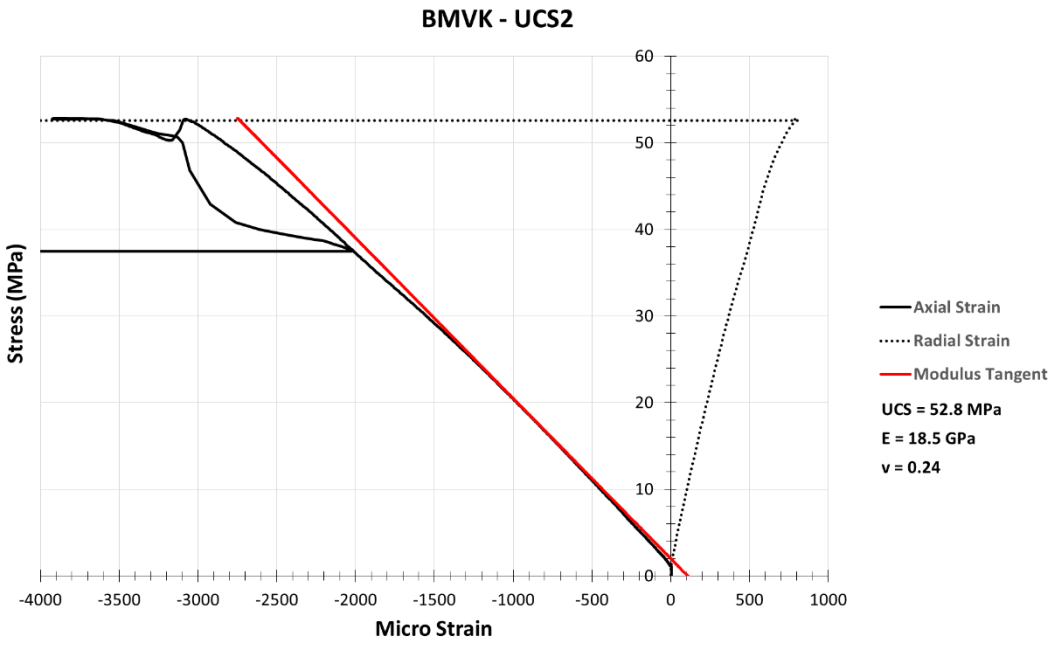

Figure C.11: BMVK – UCS2 stress vs. strain plot

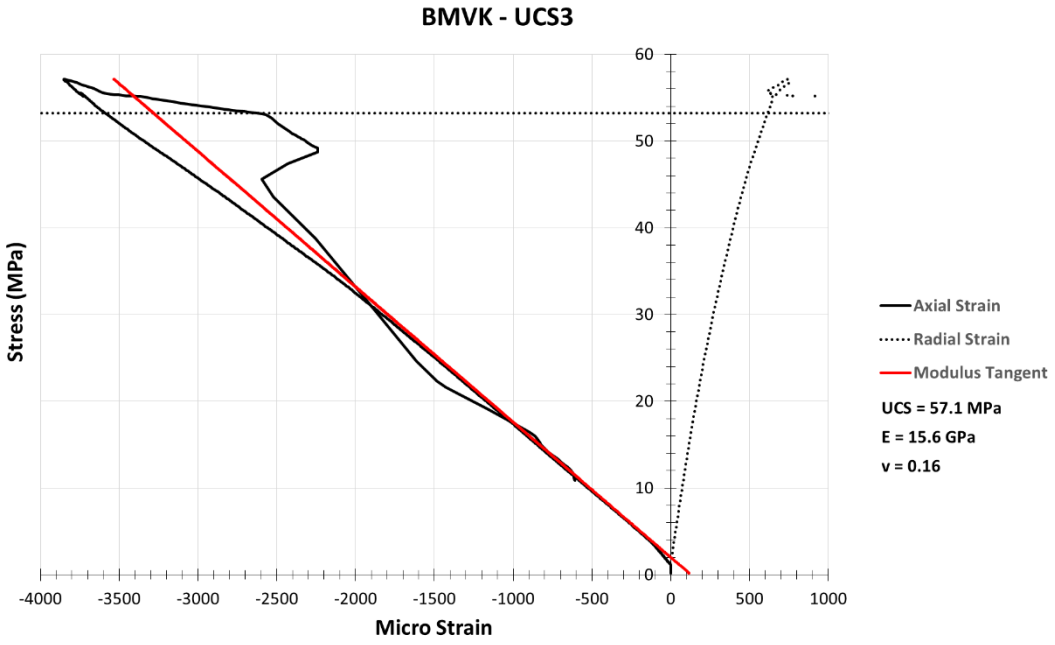

Figure C.12: BMVK – UCS3 stress vs. strain plot

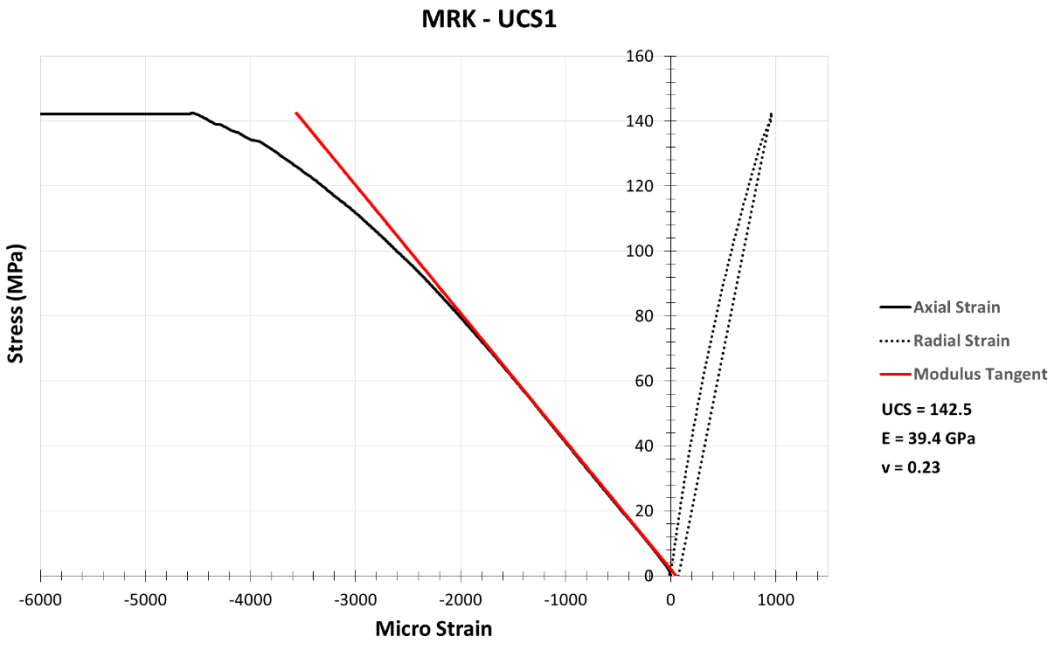

Figure C.13: MRK – UCS1 stress vs. strain plot

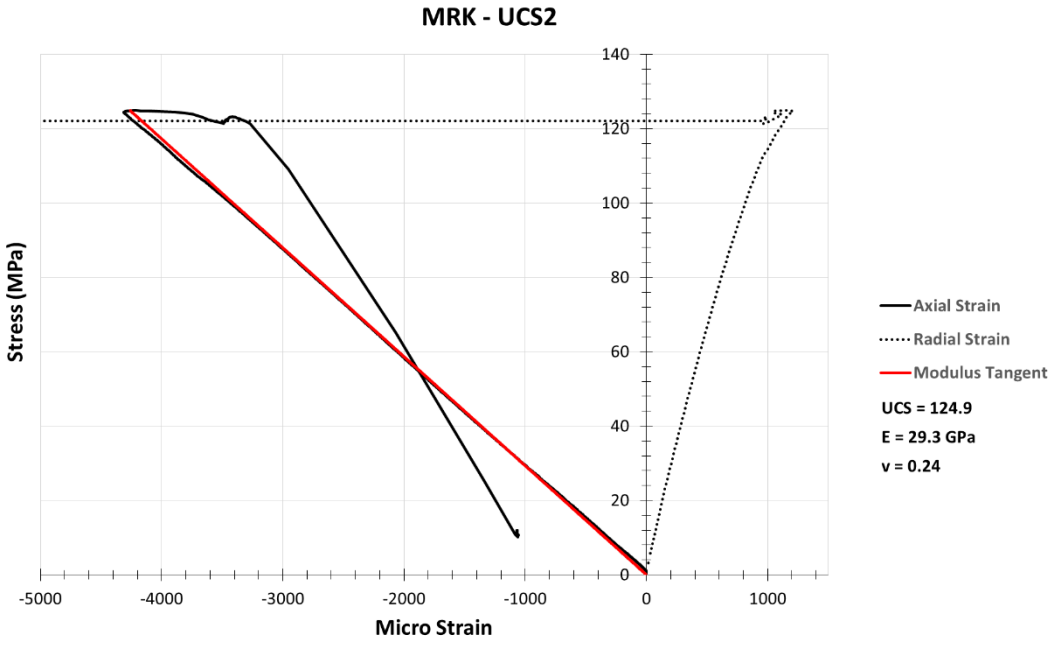

Figure C.14: MRK – UCS2 stress vs. strain plot

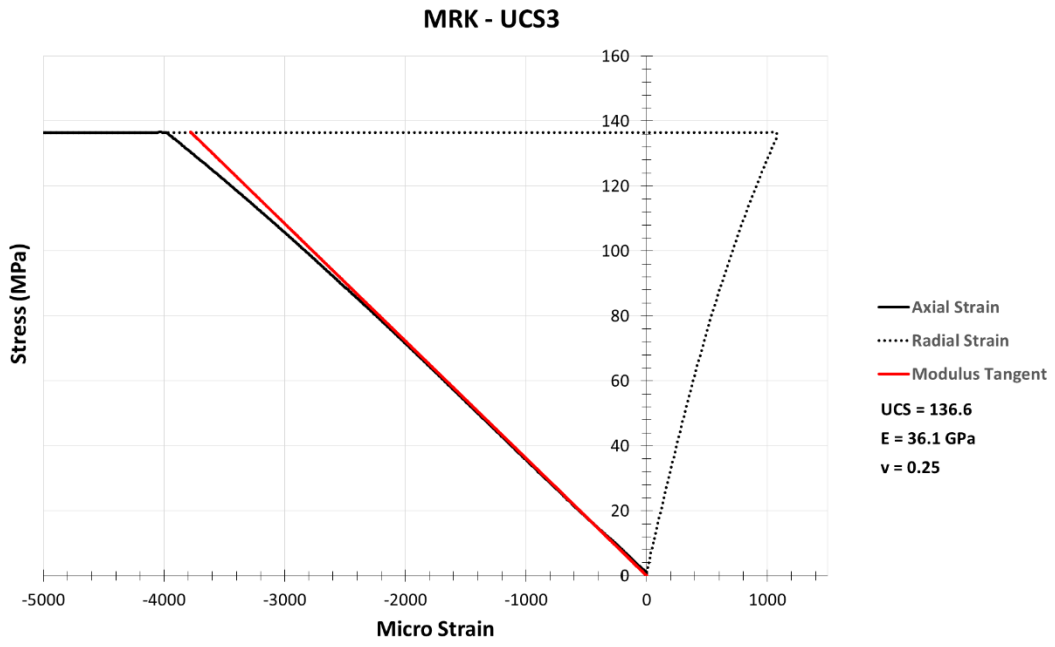

Figure C.15: MRK – UCS3 stress vs. strain plot

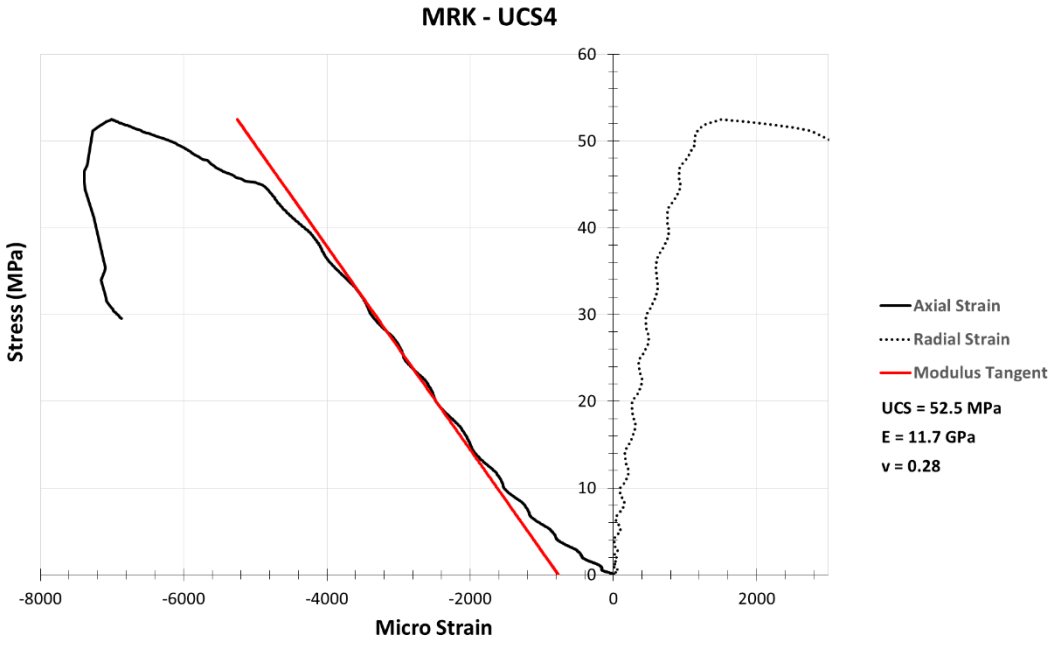

Figure C.16: MRK – UCS4 stress vs. strain plot

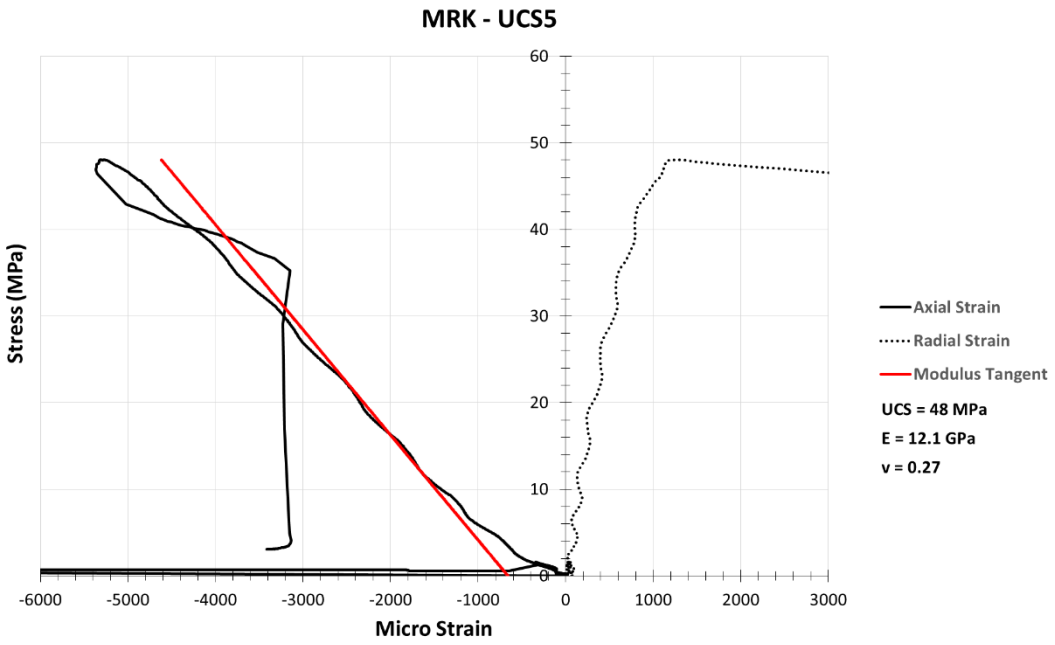

Figure C.17: MRK – UCS5 stress vs. strain plot

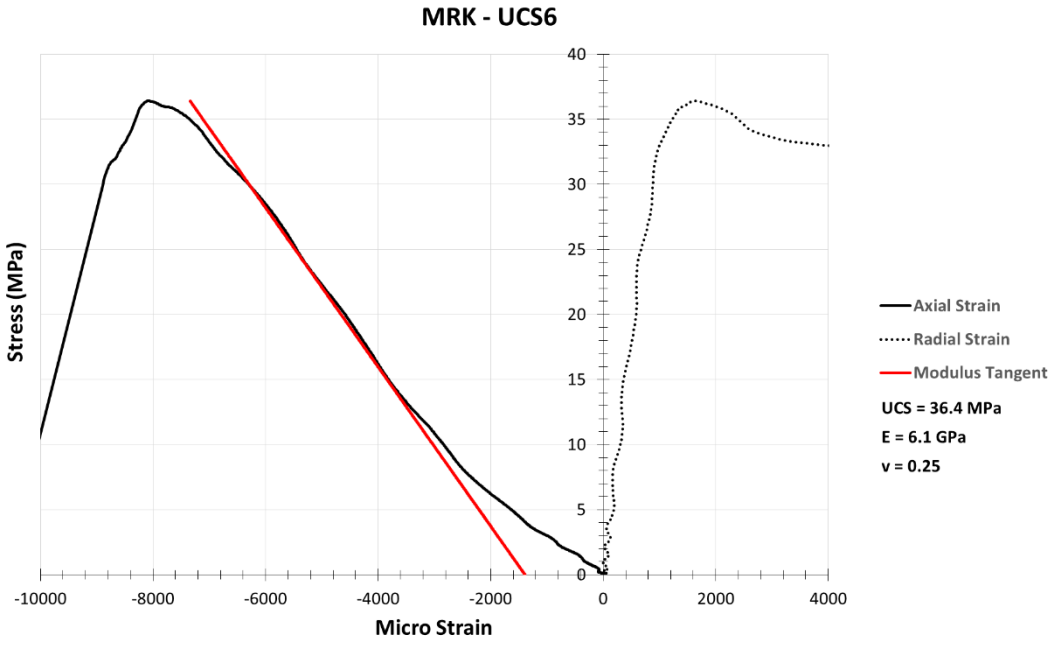

Figure C.18: MRK – UCS6 stress vs. strain plot

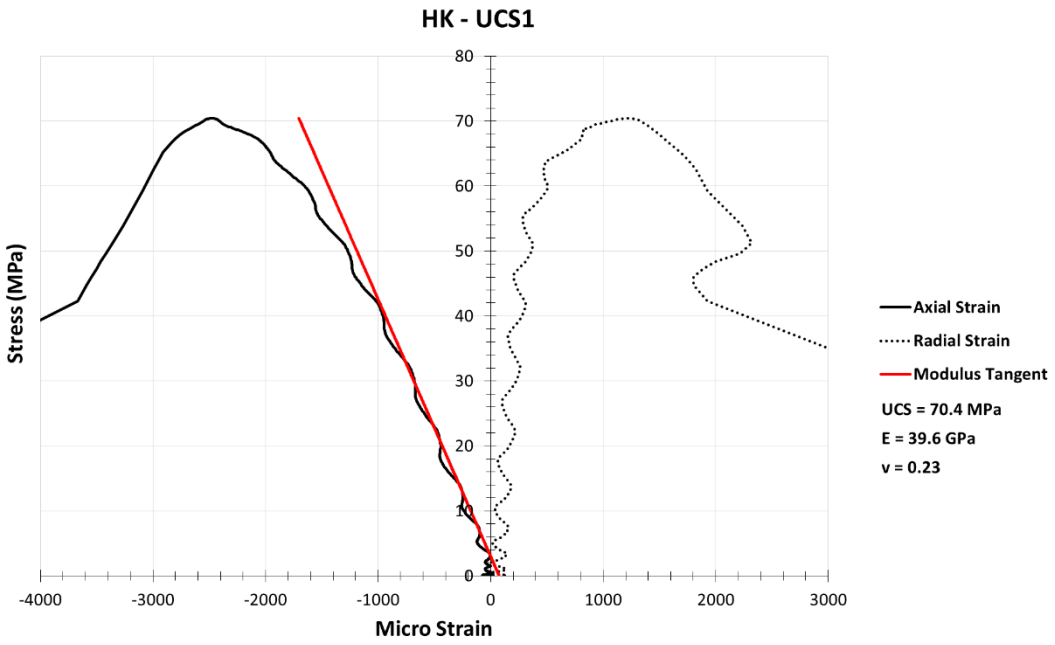

Figure C.19: HK – UCS1 stress vs. strain plot

Appendix D Hysteresis Loop Test

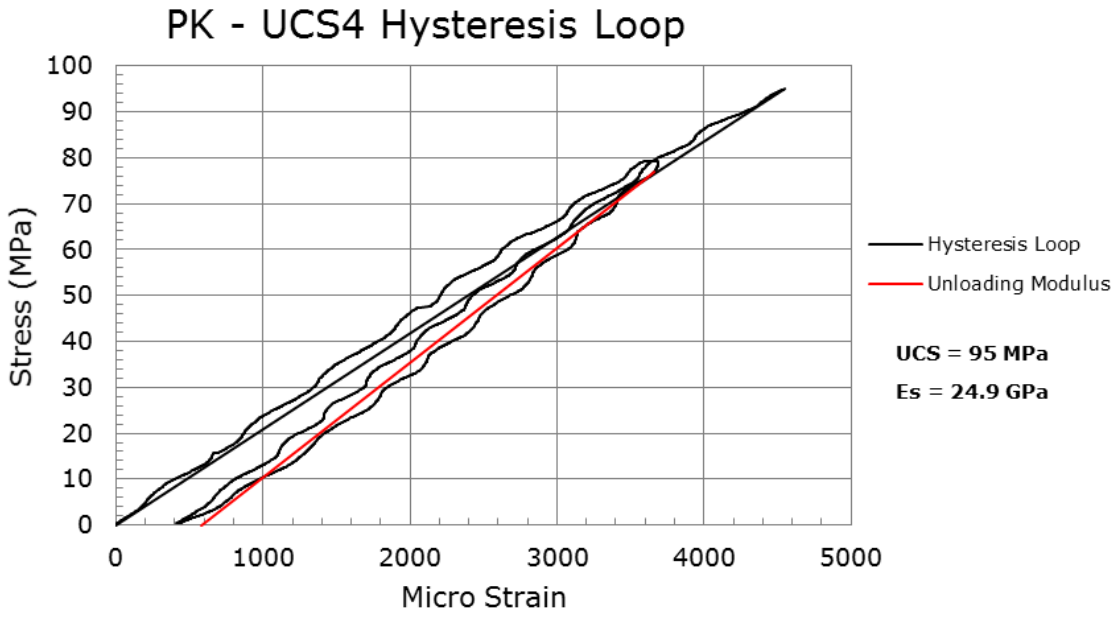

Figure D.1: PK – UCS4 hysteresis loop plot

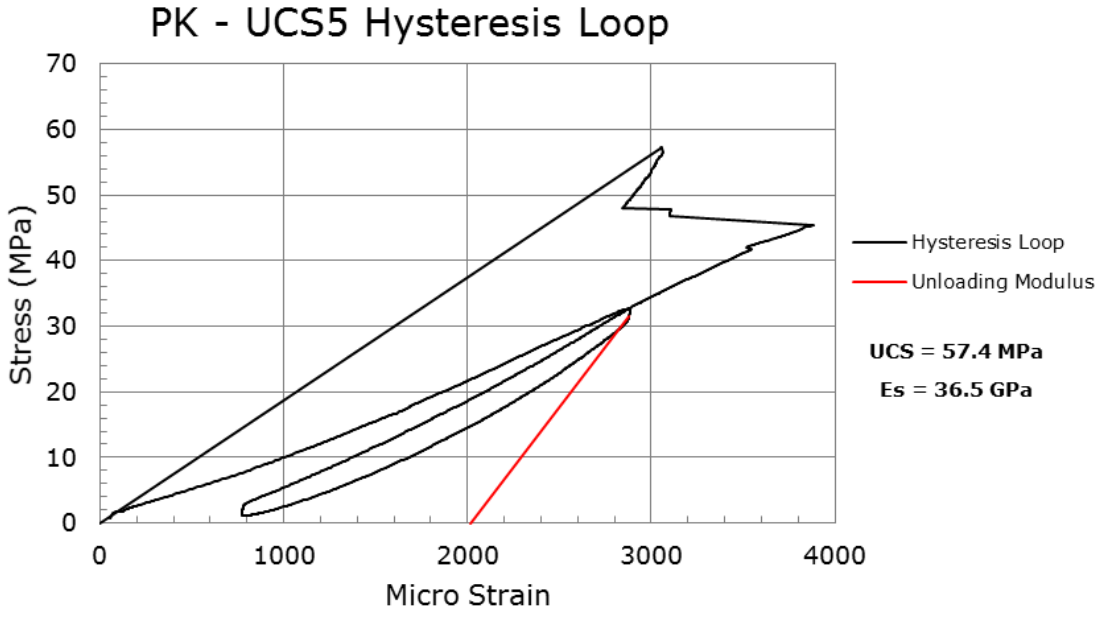

Figure D.2: PK – UCS5 hysteresis loop plot

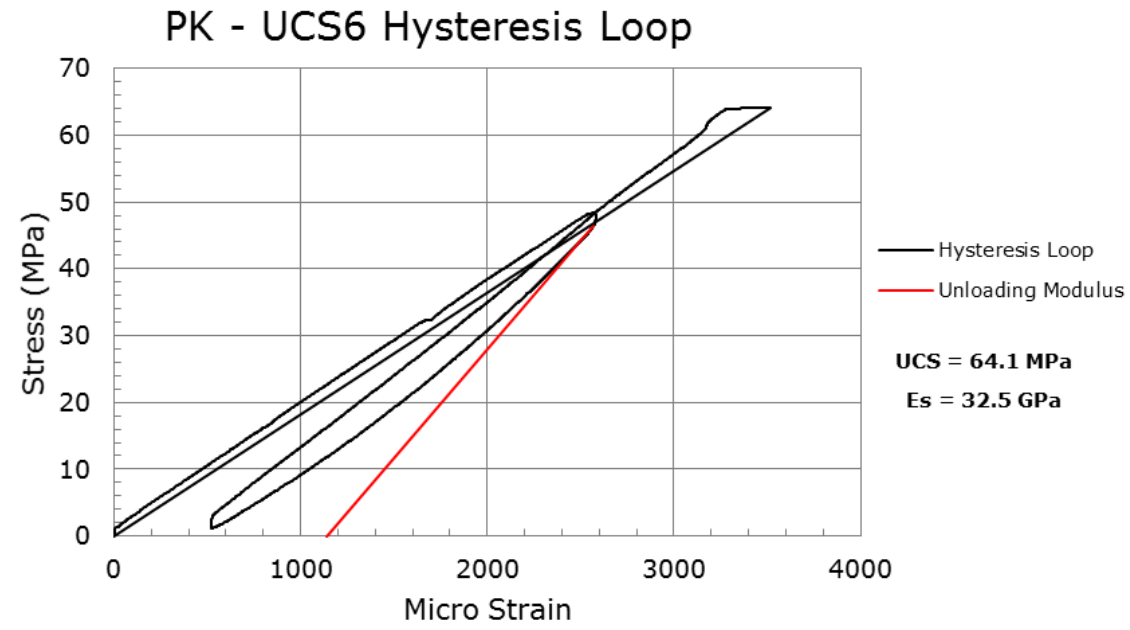

Figure D.3: PK – UCS6 hysteresis loop plot

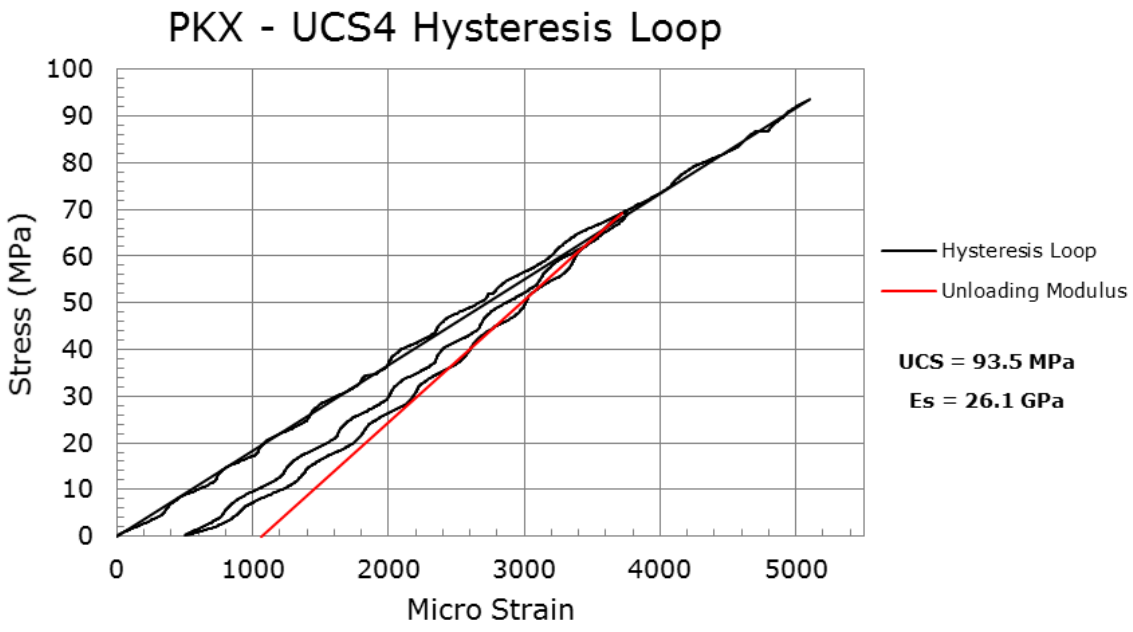

Figure D.4: PKX – UCS4 hysteresis loop plot

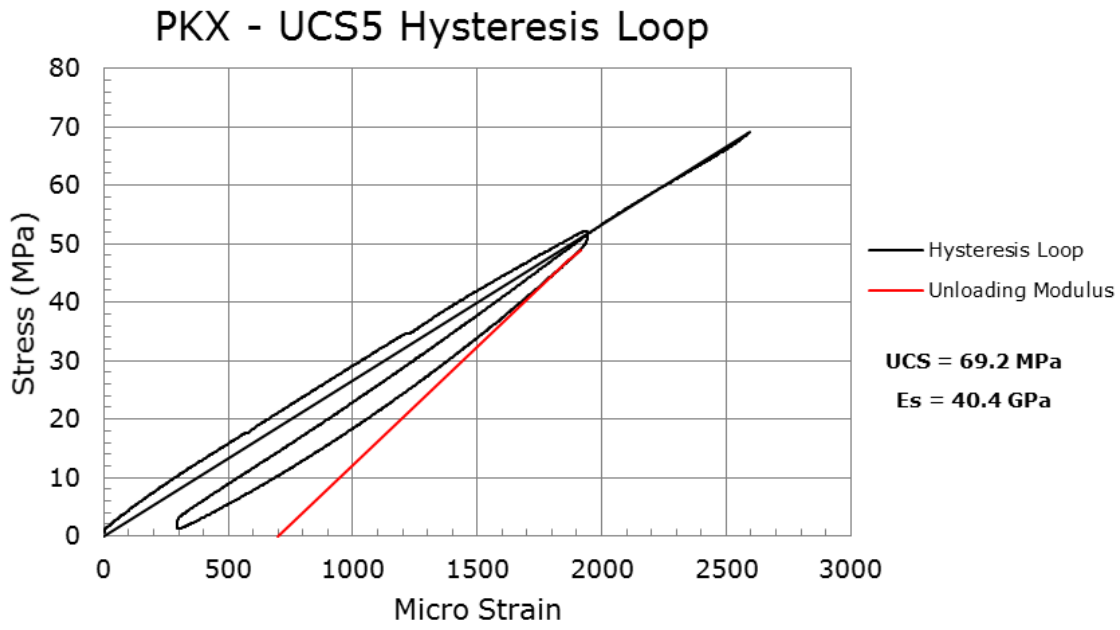

Figure D.5: PKX – UCS5 hysteresis loop plot

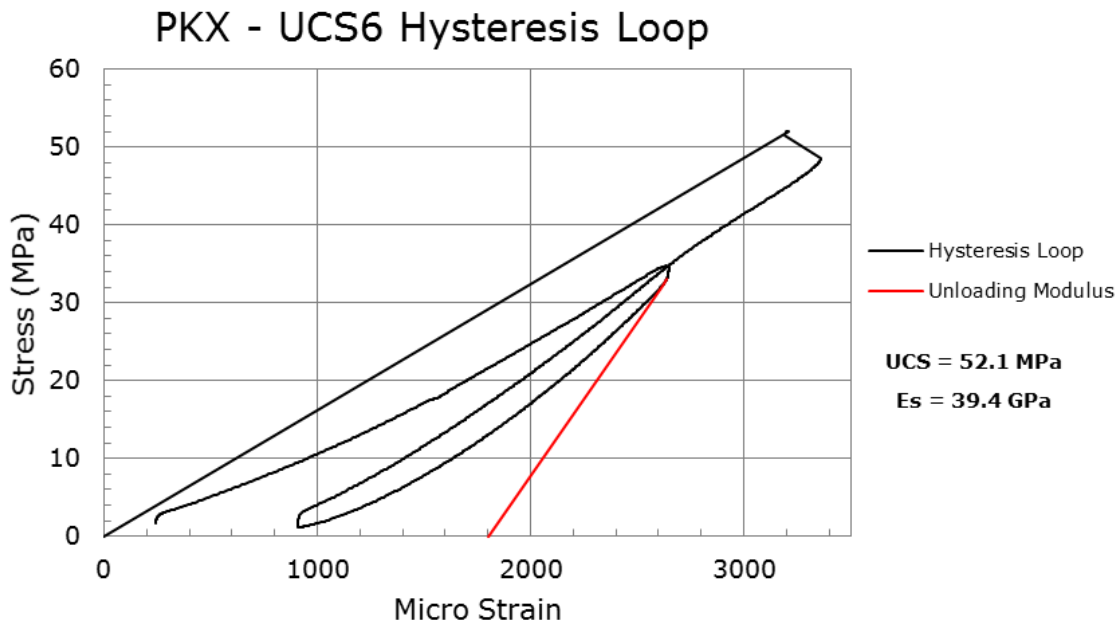

Figure D.6: PKX – UCS6 hysteresis loop plot

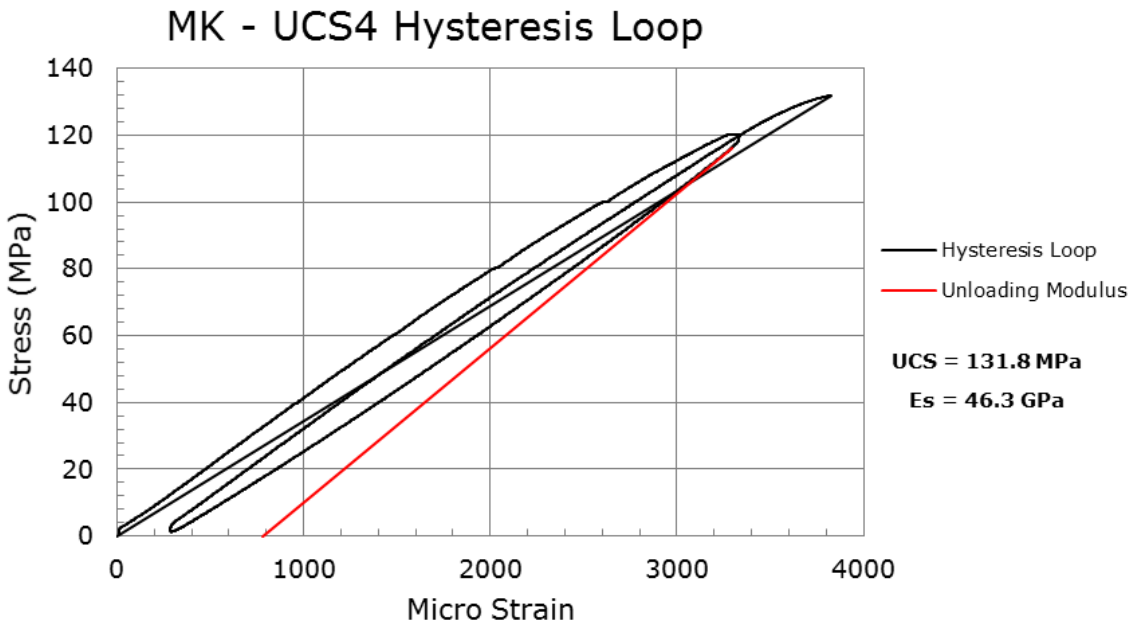

Figure D.7: MK – UCS4 hysteresis loop plot

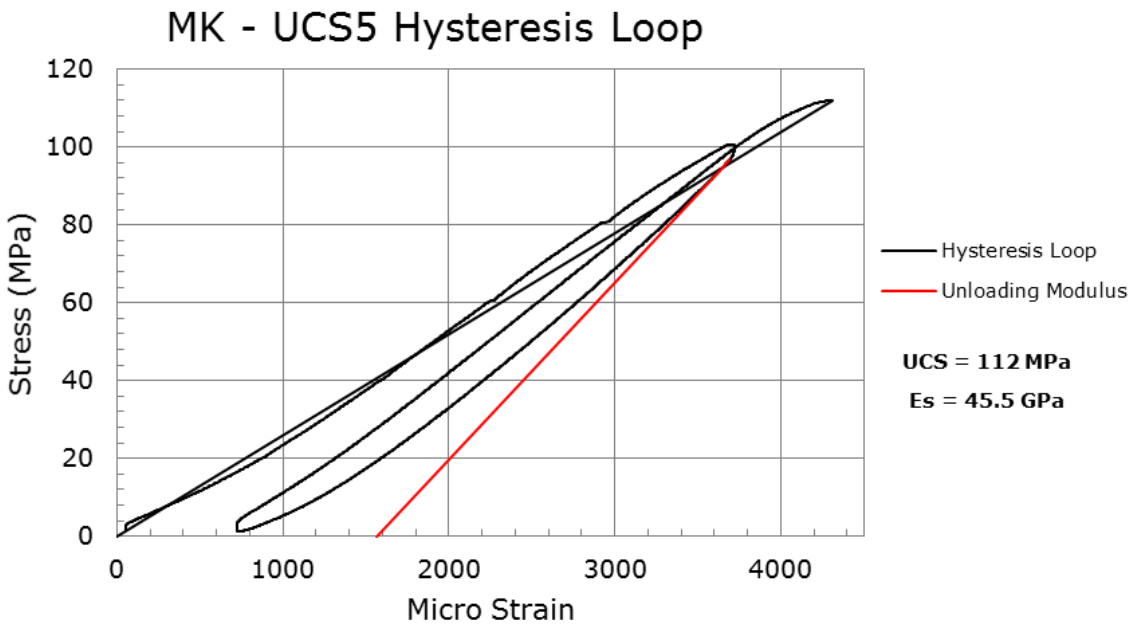

Figure D.8: MK – UCS5 hysteresis loop plot

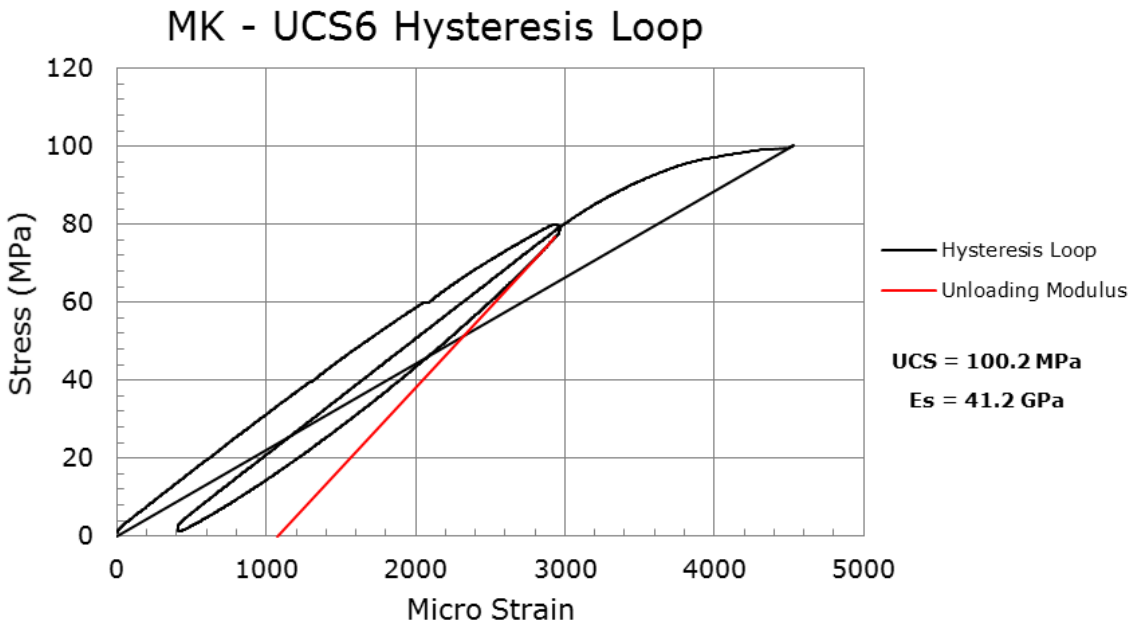

Figure D.9: MK – UCS6 hysteresis loop plot

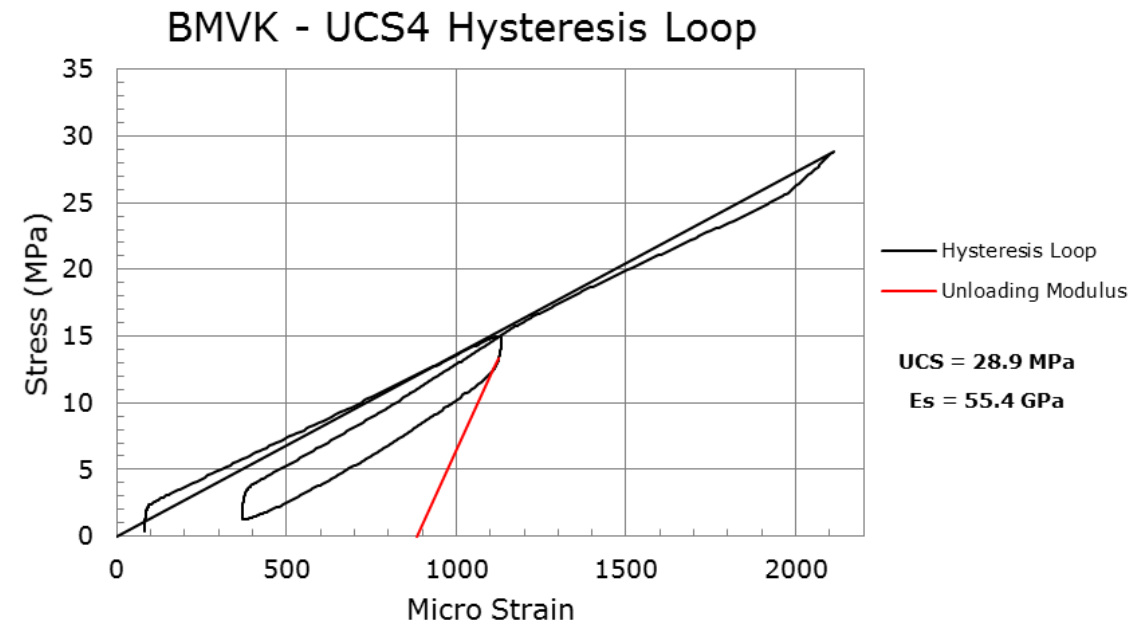

Figure D.10: BMVK – UCS4 hysteresis loop plot

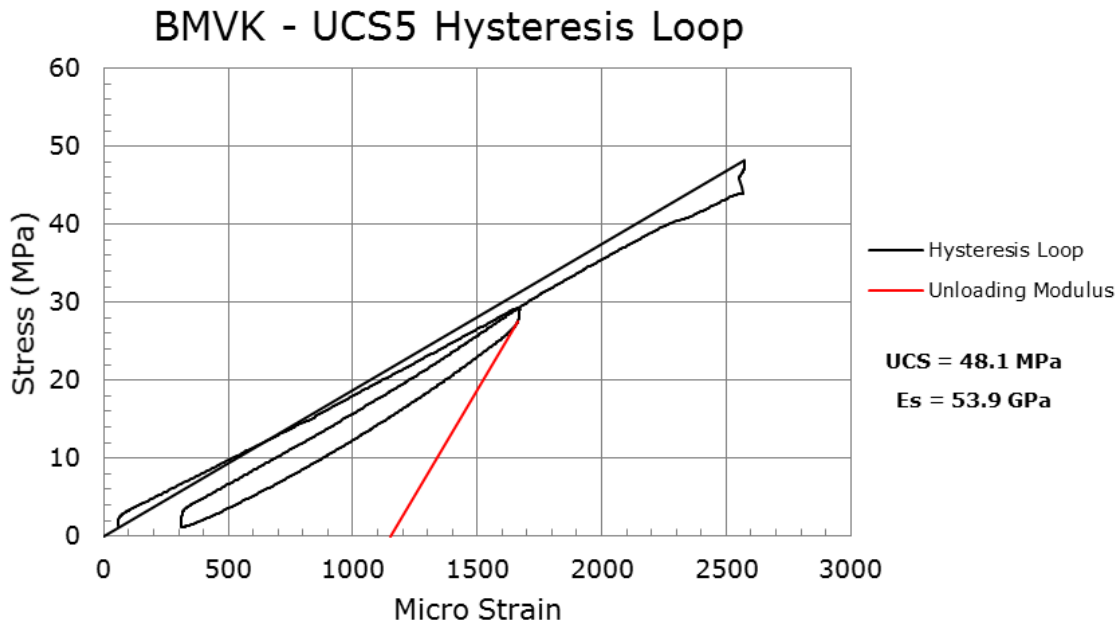

Figure D.11: BMVK – UCS5 hysteresis loop plot

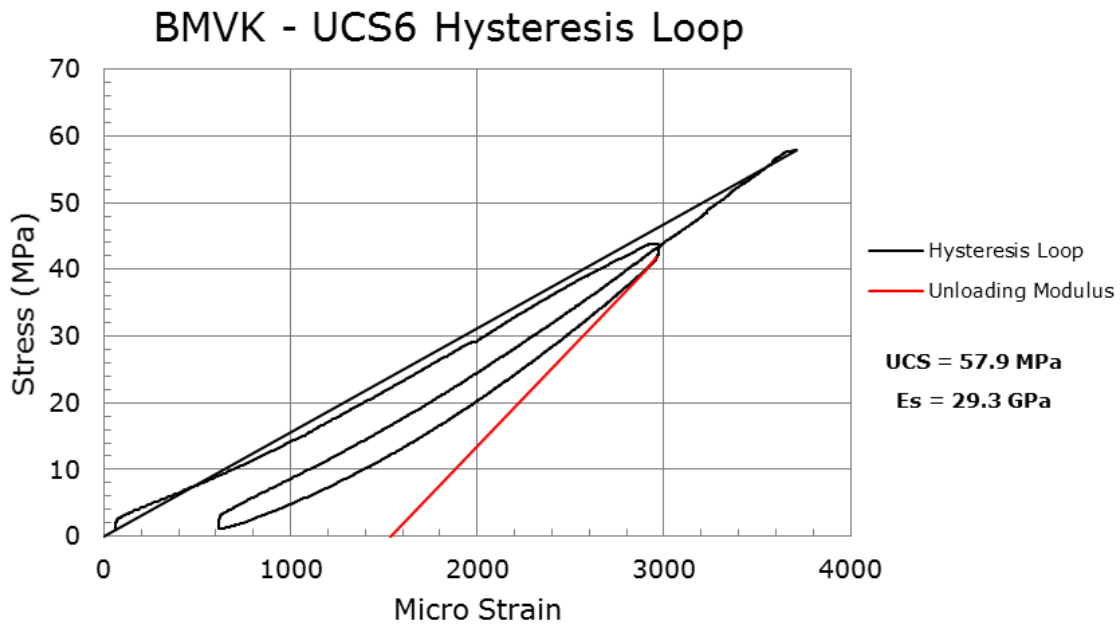

Figure D.12: BMVK – UCS6 hysteresis loop plot

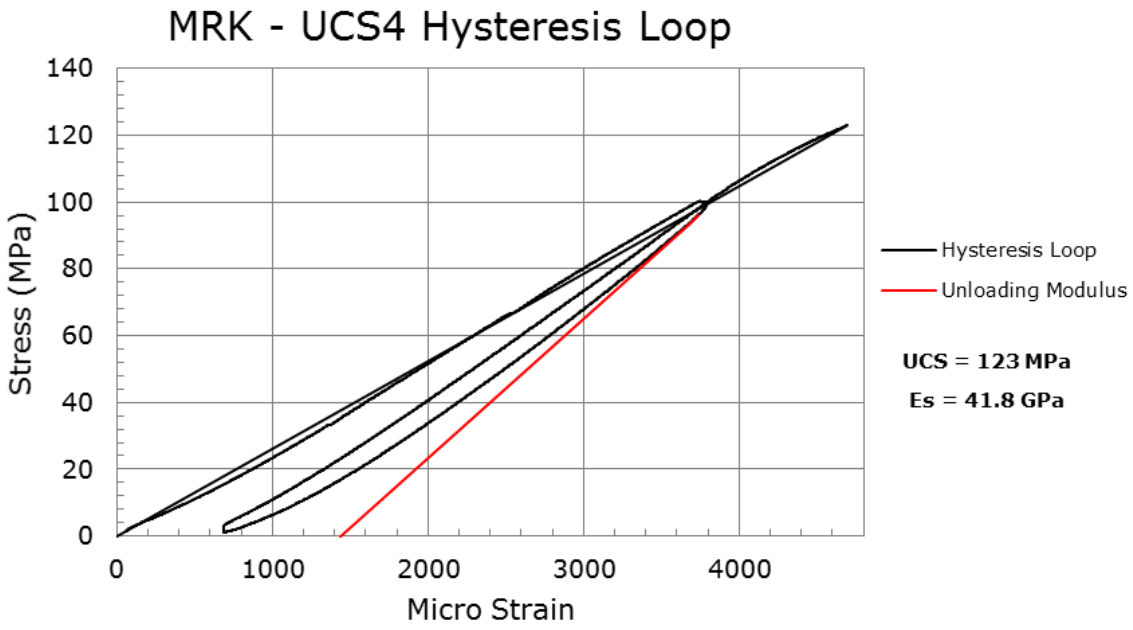

Figure D.13: MRK – UCS4 hysteresis loop plot

Appendix E Rockburst Analysis Results

Pipe	Rock Type	Sample ID	UCS (MPa)	σ_T (MPa)	E_s (GPa)	W_{ET}	SED	B Index
A154 South	PK	UCS4	95.0	3.0	24.9	3.3	181	31.4
		UCS5	57.4		36.5	1.7	45	18.9
		UCS6	64.1		32.5	2.3	63	21.2
	Average		**72.1**		**31.3**	**2.4**	**96**	**23.8**
	PKX	UCS4	93.5	3.7	26.1	3.2	168	25.1
		UCS5	69.2		40.4	2.5	59	18.6
		UCS6	52.1		39.4	1.5	34	14.0
	Average		**71.6**		**35.3**	**2.4**	**87**	**19.2**
A154 North	MK	UCS4	131.8	4.4	46.3	5.2	188	30.1
		UCS5	112.0		45.5	2.5	138	25.6
		UCS6	100.2		41.2	2.8	122	22.9
	Average		**114.7**		**44.3**	**3.5**	**149**	**26.2**
	BMVK	UCS4	28.9	3.4	55.4	1.2	8	8.5
		UCS5	48.1		53.9	2.3	21	14.2
		UCS6	57.9		29.3	2.2	57	17.1
	Average		**45.0**		**46.2**	**1.9**	**29**	**13.3**
	MRK	UCS4	123.0	3.2	41.8	3.4	181	38.6
		UCS5	-		-	-	-	-
		UCS6	-		-	-	-	-
	Average		**123.0**		**41.8**	**3.4**	**181**	**38.6**

*Tensile strength based on average from Brazilian tests

Table E.1: Summary of rockburst analysis calculations from hysteresis loops

Pipe	Rock Type	Sample ID	UCS (MPa)	σ_T (MPa)	B Index
A154 South	PK	UCS1	49.1	3.0	16.2
		UCS2	60.0		19.8
		UCS3	82.2		27.2
	Average		**63.8**		**21.1**
	PKX	UCS1	74.8	3.7	20.1
		UCS2	76.0		20.4
		UCS3	57.3		15.4
	Average		**69.4**		**18.6**
A154 North	MK	UCS1	112.6	4.4	25.7
		UCS2	79.9		18.2
		UCS3	49.5		11.3
	Average		**80.7**		**18.4**
	HK	UCS1	70.4	9.7	7.3
	BMVK	UCS1	65.1	3.4	19.2
		UCS2	52.8		15.6
		UCS3	57.1		16.9
	Average		**58.3**		**17.3**
	MRK	UCS1	142.5	3.2	44.8
		UCS2	124.9		39.2
		UCS3	136.6		42.9
	Average		**134.7**		**42.3**
	MRK	UCS4	52.5	3.9	13.5
		UCS5	48.0		12.3
		UCS6	36.4		9.3
	Average		**45.6**		**11.7**

*Grey shading indicates second set of testing
*Tensile strength based on average from Brazilian tests

Table E.2: Summary of brittleness index values from UCS tests